BENEMÉRITA UNIVERSIDAD AUTÓNOMA DE PUEBLA

INSTITUTO DE FÍSICA “LUIS RIVERA TERRAZAS”

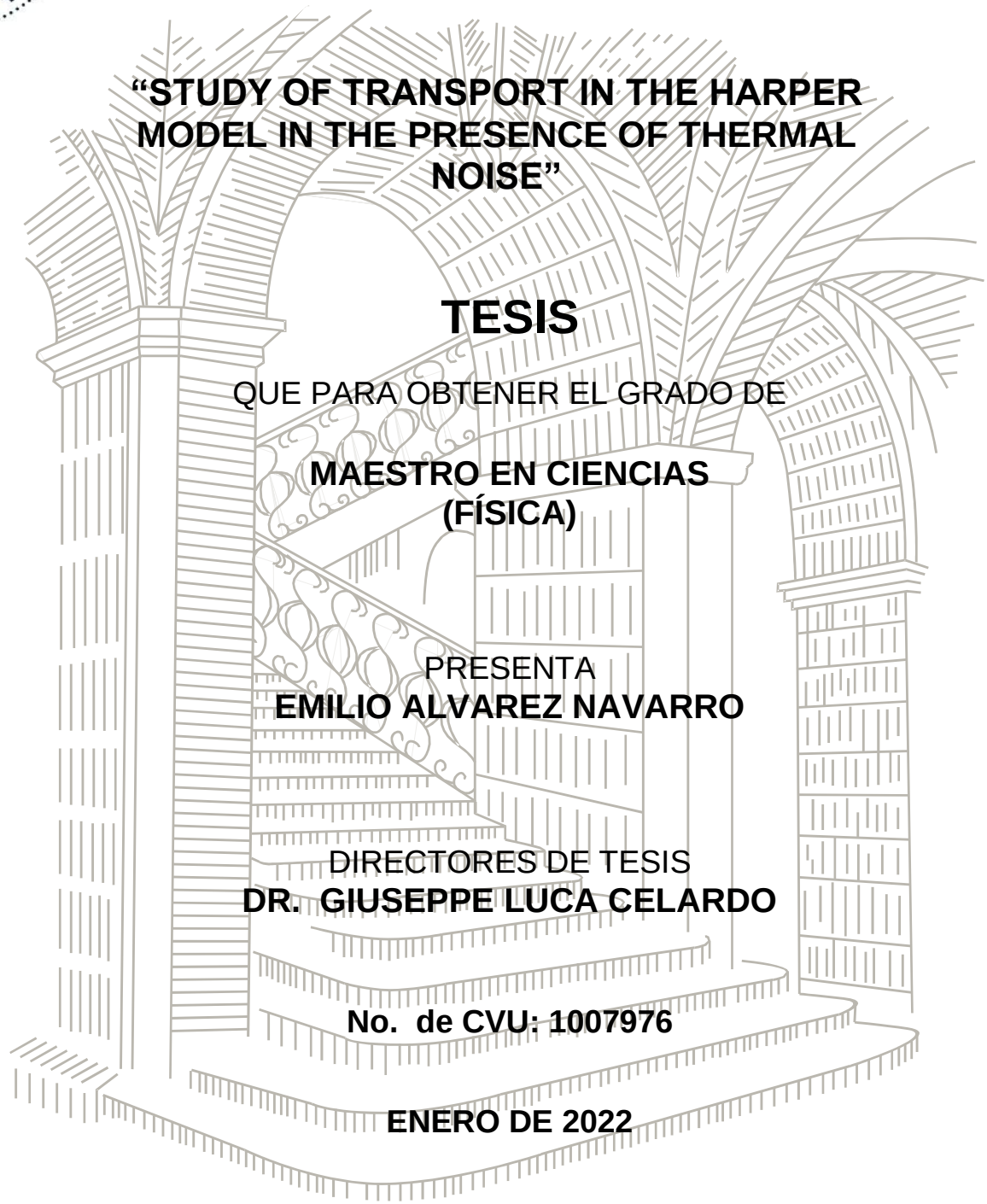

“STUDY OF TRANSPORT IN THE HARPER MODEL IN THE PRESENCE OF THERMAL NOISE”

TESIS

QUE PARA OBTENER EL GRADO DE

MAESTRO EN CIENCIAS (FÍSICA)

PRESENTA

EMILIO ALVAREZ NAVARRO

DIRECTORES DE TESIS

DR. GIUSEPPE LUCA CELARDO

No. de CVU: 1007976

ENERO DE 2022

Agradecimientos

Agradezco mis padres y hermano por su inifinito amor y apoyo a lo largo de mi vida.

Al Dr. Giuseppe Luca Celardo, al Dr. Nahum Calderón Chávez y al Dr. Francesco Mattiotti por su orientación durante el desarrollo de la inverstigación, su exigencia y consejos.

Al Consejo Nacional de Ciencia y Tecnología (CONACYT) por brindarme apoyo económico durante el tiempo que realice mis estudios.

Al Instituto de Física de la Universidad Autonoma de Puebla "Luis Rivera Terrazas" (IFUAP) por permitirme continuar con mis estudios.

A los doctores de quienes la oportunidad de aprender, en especial al Dr. Mauricio Torres Gonzalez y Dr Omar de la Peña Seaman.

A mis compañeros y amigos de maestría. En espacial a Angélica, Carlos y José Antonio.

A Majo, Raúl, Ruben, Miguel y mi Gurú, por su apoyo en todo momento.

A mis mejores amigos, esto no fue gracias a ustedes, riduculos.

Estudio del transporte en el modelo de Harper en presencia de ruido térmico
Resumen

En esta tesis se estudia el transporte cuántico del modelo de Harper en presencia de ruido térmico. El modelo Harper es un modelo paradigmático de transporte cuántico que presenta una transición metal-aislante en una dimensión. El modelo de Harper representa un salto de partículas en una cadena unidimensional con un potencial cuasi-periódico.

A lo largo de la tesis se han estudiado diferentes figuras de mérito para la eficiencia del transporte. En concreto, se ha analizado la propagación de un paquete de ondas inicialmente localizado en el centro de una cadena, se ha calculado el coeficiente de difusión mediante la expresión de Green-Kubo y se ha analizado la corriente en estado estacionario. Se utilizó una ecuación maestra de Lindblad para modelar la interacción del sistema con el entorno. En este caso, el entorno está dominado por ruido blanco no correlacionado, por lo que se utilizó la aproximación de Haken-Strobl para modelar el entorno. La corriente en estado estacionario se calculó utilizando diferentes enfoques: utilizando una ecuación maestra que incluye el bombeo y el drenaje del primer y el último sitio, utilizando una ecuación maestra para calcular el tiempo medio de transferencia y, por último, encontramos la corriente en términos del coeficiente de difusión usando la expresión de Green-Kubo.

Nuestro análisis muestra que en el régimen metálico el desfasamiento es siempre perjudicial para el transporte, mientras que en el régimen localizado el desfasamiento ayuda al transporte hasta que se alcanza un desfasamiento óptimo. La evidencia numérica obtenida en esta tesis sugieren que en la transición metal-aislante, el transporte es independiente del desfasamiento hasta un desfasamiento crítico que es independiente del tamaño del sistema. Este es el mensaje principal de esta tesis. El tamaño máximo tamaño del sistema analizado numéricamente fue diferente para cada una de las figuras de mérito consideradas. Para las propiedades que involucren el uso de la ecución maestra, el tamaño máximo del sistema fue de $N = 100$. Para el coefficiente de difussión obtenido por la expresión de Green-Kubo, el tamaño máximo del sistema fue de $N = 5 \times 10^4$. Por último, para el estudio del modelo cuando no involucra desfasamiento, el tamaño máximo del sistema fue de $N = 10^4$.

Además, hemos obtenido que en la transición metal-aislante el segundo momento

de un paquete de ondas, el cual inicialmente esta totalmente situado en el sitio central de la cadena, es independiente del desfasamiento por debajo de una fuerza de desfase crítica, y se caracteriza por un movimiento difusivo. Hemos propuesto una expresión para el coeficiente de difusión que describe adecuadamente las simulaciones numéricas, diferente a la obtenida por la expresión de Green-Kubo. En nuestra expresion, el coeficiente de difusión D en el MIT puede escribirse como $D = a^2/2\tau_{hop}$, donde a es la longitud de los eslabones de la cadena y $\tau_{hop} = \hbar/\Omega$ es el tiempo de salto determinado por el acoplamiento de salto al vecino más cercano Ω.

Study of transport in the Harper model in the presence of thermal noise
Abstract

In this thesis we study quantum transport of the Harper model in the presence of thermal noise. The Harper model is paradigmatic model for quantum transport which presents a metal-insulator transition in one dimension. The Harper model represents a particle hopping in a one dimensional chain with a quasi-periodic potential.

Throughout the thesis, different figures of merit for transport efficiency have been studied. Specifically, we analyzed the spreading of a wave packet initially localized at the center of the chain, we calculated the diffusion coefficient using the Green-Kubo expression and we have analyzed the steady-state current. A Lindblad master equation was used to model the interaction of the system with the environment. Here the environment is dominated by uncorrelated white noise, so the Haken-Strobl approximation was used to model the environment. The steady-state current was computed using different approaches: using a Master equation which includes pumping and draining from the first and the last site, using a Master equation to compute the Average Transfer Time, and finally, we found the current in terms of the diffusion coefficient using the Green-Kubo expression.

Our analysis has shown that in the metallic regime dephasing is always detrimental to transport, while in the localized regime dephasing helps transport until an optimal dephasing is reached. The numerical evidence obtained in this thesis suggests that at the metal-insulator transition, transport is independent of dephasing up to a critical dephasing which is independent of the system size. This is the main message of this thesis. The maximum system size numerically analyzed was different for each of the figure of merit considered. For the properties involving the use of the master equation, the maximum system size was $N = 100$. For the diffusion coefficient obtained by the Green-Kubo expression, the maximum system size was $N = 5 \times 10^4$. Finally, for the study of the model in absence of dephasing, the maximum system size was $N = 10^4$.

Moreover, we have shown that at the metal-insulator transition the second moment of the wave packet, which is initially fully localized on the central site of the chain, is independent of dephasing below a critical dephasing strength, and it is characterized by a diffusive motion. We have proposed an expression for the diffusion coefficient that

adequately describes the numerical simulations, different from that obtained by the Green-Kubo expression. In our proposed expression, the diffusion coefficient D at the MIT can be written as $D = a^2/2\tau_{hop}$, where a is the lattice spacing and $\tau_{hop} = \hbar/\Omega$ is the hopping time determined by the nearest neighbor hopping coupling Ω.

Contents

Chapter 1

Introduction

The phenomenon of quantum transport in the coherent regime is a centerpiece in many areas of research. Understanding the phenomenon of quantum transport from a microscopic point of view would allow us to build more efficient quantum channels of communication, more efficient sunlight harvesting systems, or design devices to transmit energy without dissipation. It is for this reason that quantum transport is studied in many scientific areas such as exciton-like devices [1], light-harvesting devices [2–7], clouds of cold atoms [8–11], mesoscopic devices [12–14], and so on. Different transport regimes can be achieved by changing the system parameters.

Quantum transport is often studied in network models, where an excitation or particle can jump from one node to another. A classic example is the Anderson model in three dimensions (3D) [15], where the nodes are distributed in a cubic lattice, and the jumps occur between neighboring nodes. If disorder is present in the system, the site energies can be random. In Anderson's 3D model, a metal-insulator transition is achieved by varying the strength of disorder in the system. In fact, below a critical value of disorder, the wave function that describes the system extends through it, and the transport can be ballistic or diffusive. For values higher than the critical value, the wave function will be localized in space, and the transport is exponentially suppressed with the size of the system.

The Anderson model was introduced approximately sixty years ago, and over the years, various experimental evidences have been reported on the phenomenon called *Anderson localization*. Furthermore, in the most realistic situations, physical systems interact with their surroundings which we usually call *environments*. These interactions can be understood as time dependent perturbations on the physical system that is being studied.

It should be noted that the interaction with different environments can dramatically modify the transport properties. In particular, we are interested in analyzing the interaction with environments that induce decoherence (dynamic noise, inelastic dispersion, etc. [1, 16]) along with dissipative environments, characterized by a few decay channels, in such a way that the excitation energy can be lost. These types of environments are found in many physical systems, such as light-harvesting complexes [2–7], cold atomic clouds [8–11], and in quantum electrodynamics in experiments with waveguides [17].

In this thesis we analyze a paradigmatic model, which presents a metal-insulator transition, similar to the Anderson 3D model: The Harper model [18, 19]. The Harper model represents a one-dimensional lattice where the site energies are not random but they vary from site to site according to a deterministic rule. In this model, particles can tunnel to the nearest neighboring sites [20].

Harper model is fascinating since it has a metal-insulator transition in 1D if the site energies are quasi-periodic, contrary to the Anderson model, where the transition occurs in 3D. In this sense, Harper's model allows us to study the relevance of the metal-insulator transition in low-dimensional systems [21, 22], allowing us to explore largest system sizes. Furthermore, this model has recently received much attention and has been experimentally implemented to test the localization of matter waves [23, 24].

In this thesis, we will study the quantum transport in the 1D Harper model in the presence of different types of environments. We will particularly focus on the interplay of decoherence, thermal noise, and the metal-insulator transition on transport.

The transport properties of the system will be analyzed using a master equation approach, similar to what has been done recently in [25]. It has been argued [26] that the metal-insulator transition is an optimal point for transport since the decoherence is not too fast as in the metal regime and, at the same time, the wave functions are delocalized, allowing optimal transport. Even though this claim has been made in the past, there is still a lack of evidence to fully support it. This project also aims to find numerical evidence to refute or verify this conjecture.

In the literature, it is possible to find papers studying similar or identical properties in models similar or identical to ours. Two examples of this are the papers [27, 28]). In both papers, the authors study transport similarly or identically in a model similar o identical to ours, but they focus on when dephasing can benefit transport. In contrast, we realize that transport in MIT is independent of dephasing. Even in FIG. 4 of [28], it is shown that

transport is independent of dephasing in MIT up to a critical dephasing. These results are consistent with our analysis. However, the authors did not discuss it in that paper.

This thesis is organized as follows: Chapter two presents the model that will be used throughout the thesis, the Harper model. Its metal-insulator transition and energy spectrum are discussed. Chapter three presents the main tool used in the thesis to model an open quantum system, the Liouvillian master equation, mentioning the dissipators used throughout the work. Chapter four presents an analysis of the transport properties of the system. The analysis is mainly based on numerical simulations, focusing on different figures of merit of transport efficiency, such as the wave packet spreading, diffusion coefficient and steady-state current. Finally, in chapter five, the conclusions and perspectives are presented.

The main result of this thesis is that, at the metal-insulator transition, the transport efficiency is independent of dephasing up to a critical value of dephasing, which is independent of the size of the system.

Chapter 2

Harper Model

The Harper model, also known as the Aubry-André model, represents a one-dimensional chain where the site energies vary according to a quasi-periodic potential in the tight-binding approximation. These structures are between ordinary periodic crystal and disordered systems. Quasi-periodicity gives rise to a range of unusual behaviors that include fractal energy spectrum, multifractal eigenstates and the possible emergence of a metal-insulator transition (MIT). This kind of structures became popular in ultracold atom experiments, in the study of disorder quantum gases, many-body localization, and Bose glasses [29].

Around 1950, Harper used his model to study how transport properties vary as a function of the ratio of hopping strength to the on-site potential energy strength. Above a critical value of this ratio, it was shown by Aubry and André that a metal-insulator transition occurs. This model has been widely studied since it mimics disordered systems of three or more dimensions, where there is also a single-particle metal-insulator transition [30].

The physics of this model is governed by the Hamiltonian:

$$H = W \sum_{i=1}^{N} \cos\left(2\pi\beta i\right) |i\rangle \langle i| + \Omega \sum_{i=1}^{N-1} \left(|i\rangle \langle i+1| + \text{h.c.}\right), \tag{2.1}$$

where the states $|i\rangle$ represent the site basis. The first term in Eq. 2.1 is an on-site potential varying with lattice site, where W is the strength of the on-site potential and β is the period. The second term in Eq. 2.1 is the tight-binding nearest-neighbor coupling contribution, where Ω is the nearest-neighbor hopping strength [20, 31]. Fig 2.1 is a sketch of the Harper

model.

In this thesis we focus our attention on the case where β is the inverse golden mean $\beta = (\sqrt{5}-1)/2$. Indeed, assigning an irrational value to β results in the model exhibiting an MIT. The transport properties are studied as a function of the ratio W/Ω.

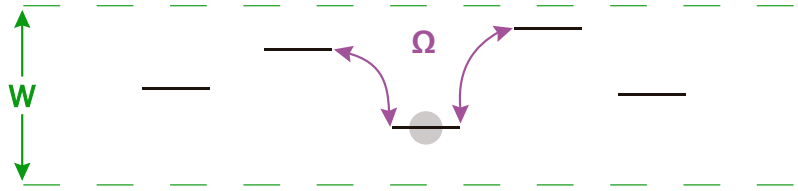

Figure 2.1: Sketch of Harper Model. The distance between the horizontal lines represent the amplitude of the on-site potential W. Here, Ω is the hopping between nearest-neighbor sites. Arrows indicate the hopping paths available for an excitation (gray circle).

2.1 Metal-Insulator Transition

A crystal with an incommensurate modulation does not possess translational symmetry. However, unlike a disordered solid, it possesses lengths over which it almost repeats. Thus, an incommensurate crystal presents an intermediate case between an ordered and a disordered solid. It has been shown that within the one-dimensional one-band tight-binding model, with incommensurate modulation, there is an MIT at critical ratio of the on-site potential and tunneling coupling $W/\Omega = 2$. This means that all the eigenfunctions are localized for $W/\Omega > 2$, while in the other extreme, all the energy eigenfunctions become extended [32] for $W/\Omega < 2$.

The MIT can be studied by analyzing the participation ratio (Pr). The Pr is useful to quantify the delocalization of eigenfunctions.

The Pr for the $|E_n\rangle$ eigenstate is defined as

$$Pr = \left(\sum_{i=1}^{N} | \langle i|E_n\rangle |^4 \right)^{-1}, \tag{2.2}$$

that measures the number of basis states over which a given state has significant support. The Pr lies in the range 1 to N, where 1 indicates a perfectly localized state and N indicates a perfectly delocalized state [33]. Localized states are characterized by a Pr which is independent of the system size, while delocalized states are characterized by a Pr which increases linearly with the system size.

Figure 2.2 shows the average of the Pr over all the eigenstates as a function of W/Ω for different values of N. This figure is obtained from the diagonalization of Eq. 2.1. Using Eq. 2.2, we obtained the Pr of each eigenstates. Then we take the average Pr for each value of W/Ω. We note that Fig. 2.2 indicates that for $W/\Omega < 2$ the value of $\langle Pr \rangle$ increases with N, while for $W/\Omega > 2$ the value of $\langle Pr \rangle$ is independent of N. This means that for values of $W/\Omega < 2$ the model exhibits delocalized behavior, while for values of $W/\Omega > 2$ the model exhibits localized behavior. The main message of this figure is that for $W/\Omega = 2$, the system exhibits the MIT, which is independent of the system size.

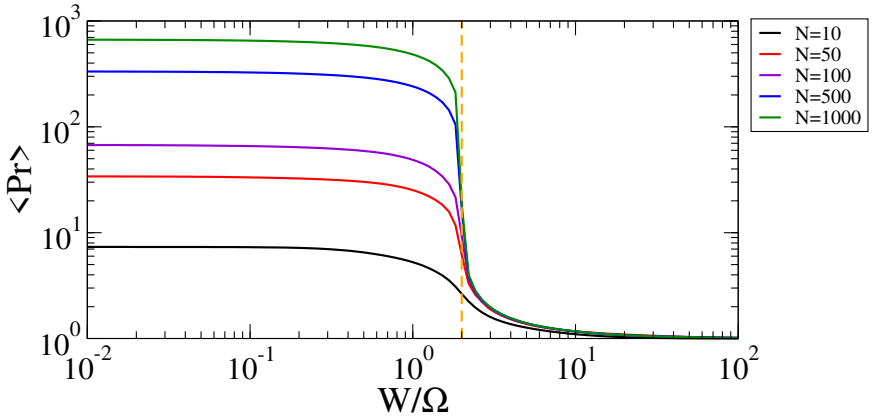

Figure 2.2: Average of the participation ratio over all eigenstates as a function of W/Ω of the Harper Model for different values of N. We obtain the figure taking the average of the Pr for all eigenstates using the Eq. 2.2. In the metallic regime ($W/\Omega < 2$), the eigenfunctions are extended and the Pr is proportional to N. In the insulating regime $W/\Omega > 2$, the eigenfunctions are localized and the Pr tends to one and it is independent of N. The parameters in this figure are: $\beta = (\sqrt{5}-1)/2$ and $\Omega = 1cm^{-1}$.

Another way to analyze the MIT is to consider the distribution of the Log(Pr) of the eigenstates. Figure 2.3, we can see how the distribution of the Log(Pr) of the eigenstates changes for different values of the ratio W/Ω for $N = 10^3$. Panel (a) is for $W/\Omega = 0$. Here, all eigenstates have the same value close to N. This means that the eigenstates are extended. In panel (b), the case $W/\Omega = 1$ is shown. We are still in the metallic phase. Panel (c)

corresponds to the MIT ($W/\Omega = 2$). The distribution of Log(Pr) is broader. Panel (d) is for $W/\Omega = 20$. Here, the distribution of Log(Pr) is very broad and most of the states have a Pr close to 0. This means that the eigenstates are localized. These results are congruent with the results shown in Fig. 2.2, where in the metal regime, the eigenstates are extended, and in the insulating regime, the eigenstates are localized.

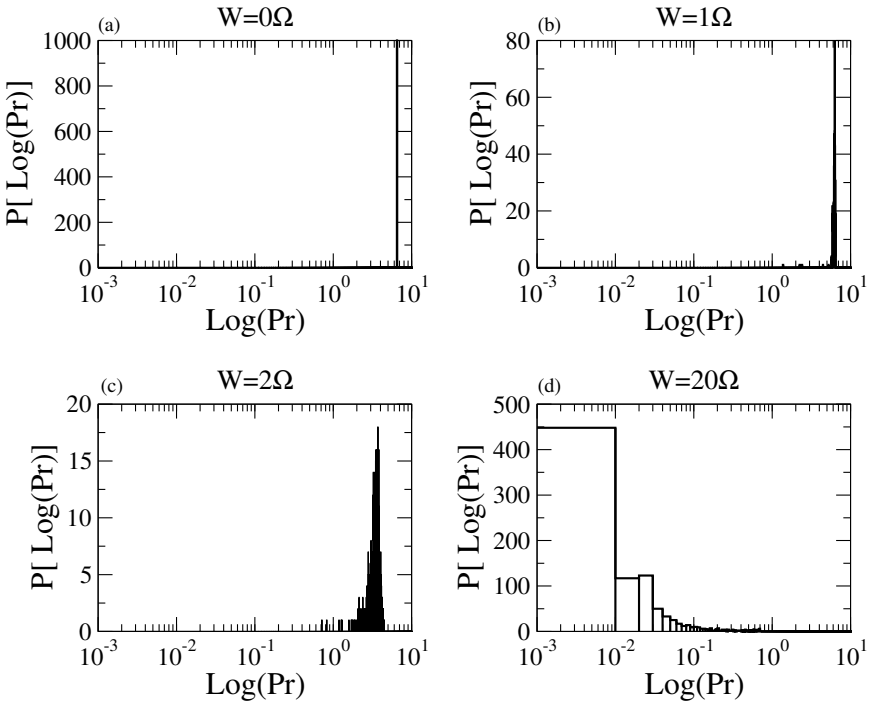

Figure 2.3: Distribution of the logarithm of the participation ratio of the eigenstates. The panels are organized for different values of W/Ω. In panel (a) is for $W/\Omega = 0$; In panel (b) is for $W/\Omega = 1$; metal regime. In panel (c) correspond to MIT $W/\Omega = 2$. Panel (d) is for $W/\Omega = 20$; insulating regime. The parameters in this figure are: $\beta = (\sqrt{5}-1)/2$, $N = 10^3$, and $\Omega = 1cm^{-1}$.

To see where the MIT occurs in the Harper model, we can also study the standard deviation σ of the Log(Pr). We use the Log(Pr) instead of Pr because the distribution of the Pr is very broad in the localized phase. Figure 2.4 shows σ : Log(Pr) as a function of W/Ω for different values of N. To obtain the data in Fig. 2.4 we diagonalize Eq. 2.1 to obtain the eigenstates. Using Eq. 2.2, we obtain the Ln(Pr) of each eigenstate in order to calculate the variance. Figure 2.4 shows that the maximal variance occurs at $W/\Omega = 2$.

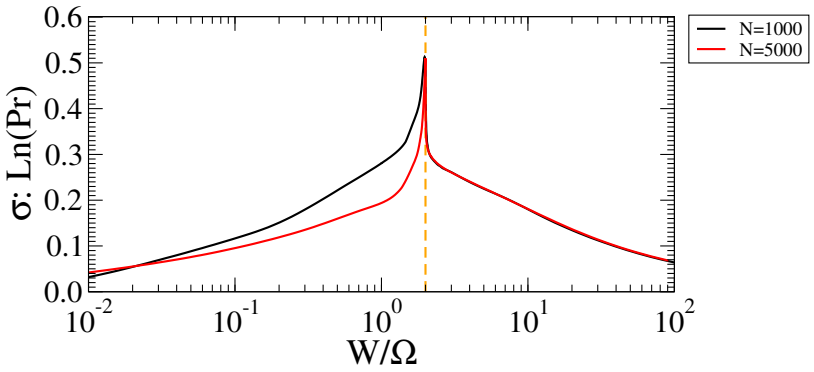

Figure 2.4: The variance of the Ln(Pr) as a function of W/Ω for different values of N. The vertical dash line marks where the MIT occurs. The value at which MIT occurs is independent of the size of the system. Moreover, the larger the system, the better this feature can be appreciated. The parameters in this figure are: $\beta = (\sqrt{5}-1)/2$ and $\Omega = 1cm^{-1}$.

2.2 Energy spectrum

Figure 2.5 shows the energy spectrum of the Harper model at the MIT as a function of the parameter β. To obtain Fig. 2.5, we solve Eq. 2.1 for $N = 2 \times 10^3$, there by obtaining 2×10^3 eigenvalues. This is done for different values of β. We choose 10^3 values of β between zero and one. Figure 2.5 gives a fractal pattern known as Hofstadter's butterfly, which has been well studied because it describes the quantum physics of an electron moving on a two-dimensional square lattice in the presence of a transverse magnetic field [34]. In particular, the vertical dash red line refers to the value of β as the inverse golden mean which we are focusing on.

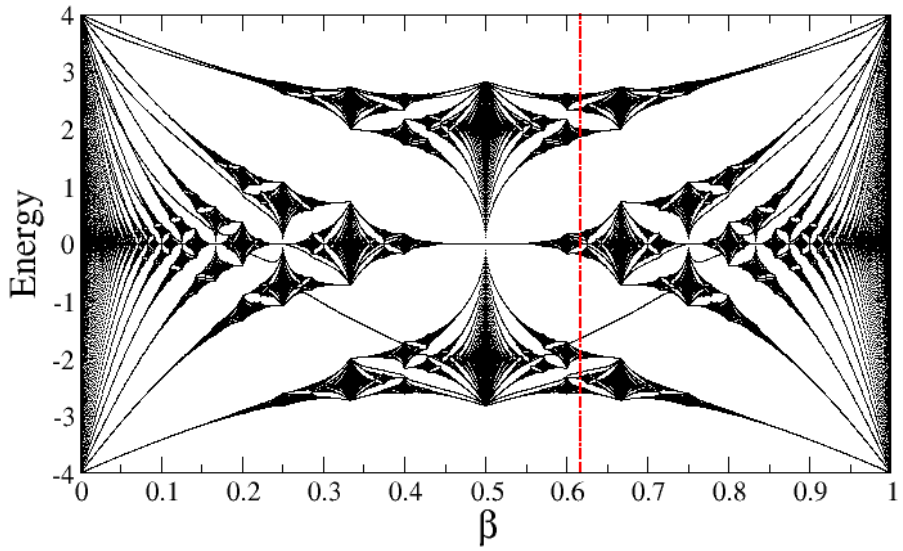

Figure 2.5: The energy spectrum of the Harper model as a function of β at $W/\Omega = 2$ for a system size $N = 2 \times 10^3$. The vertical dash line marks the inverse golden ratio ($\beta = (\sqrt{5}-1)/2$). This figure is a fractal known as the Hofstadter's butterfly [34]. The parameters in this figure are: $N = 2 \times 10^3$, $W = 2cm^{-1}$ and $\Omega = 1cm^{-1}$.

Chapter 3

Master Equation

In open quantum systems, the whole system is divided into the system of interest and the environment. Open quantum systems techniques are vital to many studies in physics, such as quantum optics, quantum information, quantum biology, and so on [35, 36]. To obtain the dynamics of the system of interest under the effect of its interaction with the environment, the Lindblad master equation is used in this thesis, which is defined as

$$\frac{\partial \rho}{\partial t} = -\frac{i}{\hbar}[H, \rho] + \mathcal{D}[\rho] \equiv \mathcal{L}[\rho]\,, \tag{3.1}$$

where H is the Hamiltonian (see Eq. 2.1), ρ is the density matrix and $\mathcal{D}$ refers to the dissipator, which represents the interaction of the system with the environment, while the symbol $\mathcal{L}$ refers to the Liouvillian superoperator. The commutator in the equation corresponds to a coherent time evolution according to H [37].

Using the Lindblad master equation, the solution for the density operator is always a positive-definite operator ρ, i.e., no negative probabilities occur, and the trace of ρ is time-independent and equal to one [38].

The general form to write $\mathcal{D}$ of the Eq. 3.1 is

$$\mathcal{D} \equiv \sum_i \frac{\gamma_i}{\hbar}[L_i \rho L_i^\dagger - \frac{1}{2}\{L_i^\dagger L_i, \rho\}]\,, \tag{3.2}$$

where the operators L_i are Lindblad operators, representing the coupling of the environment with the system, and γ_i is the amplitude of the dissipator.

3.1 Haken-Strobl Pure Dephasing

In this thesis, the system interaction with the environment induces white-noise fluctuations of the site energies. This kind of perturbation is well captured by the Haken-Strobl model pure dephasing. The Haken-Strobl pure-dephasing model is a simplified but practical model that has been used in quantum optics, condensed-matter physics, quantum information science, and physical chemistry [39].

The Haken-Strobl pure-dephasing model describes the dynamics resulting from having the site energies ϵ_i fluctuating in time with white noise correlations

$$\langle \epsilon_i(t)\epsilon_j(t')\rangle = \frac{\gamma_\phi}{\hbar}\delta_{ij}\delta(t-t')\,, \tag{3.3}$$

where $\delta_{i,j}$ being the Krönecker delta and γ_ϕ is the dephasing strength. In order to obtain the Haken-Strobl model, we need to make some assumptions. First, we assumed that fluctuations at different sites are uncorrelated. Second, we assumed that the phonon correlation time is small compared to the system time scales. Finally, the correlator is assumed to be site independent, so all the sites experience the same dephasing strength to the environment [40].

The Haken-Strobl model is a dephasing term that dampens all the off-diagonal ρ through the generators $L_i = |i\rangle\langle i|$ at a rate γ_ϕ [39]. Substituting L_i and γ_ϕ in Eq. 3.2, we obtain

$$\mathcal{L}_\phi[\rho] = \frac{\gamma_\phi}{\hbar}\sum_{i=1}^{N}\left[|i\rangle\langle i|\,\rho\,|i\rangle\langle i| - \frac{1}{2}|i\rangle\langle i|\,\rho - \frac{1}{2}\rho\,|i\rangle\langle i|\right]. \tag{3.4}$$

The damping rate of the ρ_{ij} element of the density matrix on the site basis is thus

$$\langle i|\mathcal{L}_\phi[\rho]|j\rangle = \frac{\gamma_\phi}{\hbar}(1-\delta_{i,j})\rho_{i,j}\,, \tag{3.5}$$

while the site-vacuum dephasing terms are

$$\langle 0|\mathcal{L}_\phi[\rho]|j\rangle = -\frac{\gamma_\phi}{2\hbar}\rho_{0,j}\,. \tag{3.6}$$

3.2 Pumping and Draining

In order to analyze the excitation current flowing through a chain, we add two dissipators to Eq. 3.2, the pumping and draining. The generators of pumping and draining

have the form $L_i = \sqrt{\gamma_p/(2\hbar)}\,|1\rangle\langle 0|$ and $L_i = \sqrt{\gamma_d/(2\hbar)}\,|0\rangle\langle N|$, respectively. The form of this new dissipators are

$$\mathcal{L}_p[\rho] = \frac{\gamma_p}{\hbar}\left(|1\rangle\langle 0|\,\rho\,|0\rangle\langle 1| - \frac{1}{2}\,|0\rangle\langle 0|\,\rho - \frac{1}{2}\rho\,|0\rangle\langle 0|\right) \tag{3.7}$$

$$\mathcal{L}_d[\rho] = \frac{\gamma_d}{\hbar}\left(|0\rangle\langle N|\,\rho\,|N\rangle\langle 0| - \frac{1}{2}\,|N\rangle\langle N|\,\rho - \frac{1}{2}\rho\,|N\rangle\langle N|\right). \tag{3.8}$$

The effect of these two new dissipators is as follows: an excitation starts in $|0\rangle$, which goes to the first site ($|1\rangle$) of the chain through the pumping dissipator. The excitation passes through the entire chain to the last site ($|N\rangle$) and returns to $|0\rangle$ through the drain dissipator. In this way, we generate a current.

Finally, placing all the above terms in the Lindblad master equation, the following form is obtained

$$\mathcal{L}[\rho] = -\frac{i}{\hbar}\left[H\rho - \rho H\right] + \mathcal{L}_\phi[\rho] + \mathcal{L}_p[\rho] + \mathcal{L}_d[\rho]\,. \tag{3.9}$$

Figure. 3.1 shows a sketch of the complete system, which consists of the Harper Model (see Eq. 2.1) that has its chain edges connected to the vacuum state (see Eq. 3.7 and Eq. 3.8) and it is interacting with the environment (see Eq. 3.4).

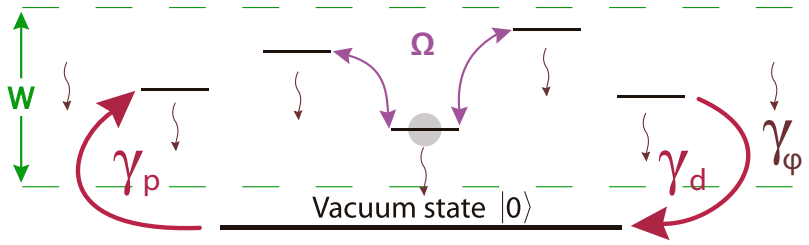

Figure 3.1: Sketch of the complete system, consisting of the Harper Model and three dissipators: Haken-Strobl, pumping and draining. The dashed green lines represent the value of W. The purple arrows indicate the tunneling amplitude Ω between the nearest neighbor sites. The brown arrows represent dephasing γ_ϕ generated by the environment. The red arrows indicate the excitation pumping γ_p and draining γ_d.

Chapter 4

Transport properties

The results obtained in this thesis regarding transport efficiency are presented in this chapter. We analyze several figures of merit for transport efficiency to understand better how transport is affected by the environment. We divide the obtained results into five sections. Moreover, we add Appx A and Appx B, where we talk about the purity and the coherence length during the transport.

In the first section, we discuss the spreading of the wave function. We can visualize how the probability of finding an excitation along a one-dimensional chain changes through time for different values of W/Ω and dephasing.

In the second section, we define the main transport regimes of a quantum system. In the third section, we discuss how to obtain the diffusion coefficient using the Green-Kubo expression. We also discuss the behavior of the diffusion coefficient as a function of dephasing and W/Ω for different system size.

In the fourth section, we discuss the dynamics of the spreading of a wave packet and split it into two subsections: spreading with zero dephasing and spreading with dephasing. In the first subsection, we derive ballistic and diffusive expressions that describe the spreading motion of a wave packet with zero dephasing. In the second subsection, we analyze the spreading of a wake packet in presence of dephasing using the wave packet variance. Furthermore, we verify the accuracy of the diffusion coefficient of the Green-Kubo expression.

In the fifth section, we analyze the steady-state current of the system. We also split this section into four subsections. To begin, in the first subsection, we start with the Master Equation method. There, we exhibit the typical behavior of the steady-state

current as a function of dephasing. After that, in the second subsection, we show how to construct the steady-state current from the average transfer time in absences of dephasing and compare the results with the results of the Master Equation. In the third section, analogously, we construct the steady-state current of the whole system and compare the results with the results of the Master Equation. Last, in the fourth subsection, we use a heuristic method based on the diffusion coefficient to obtain the steady-state current in terms of the coefficient obtained by the Green-Kubo expression.

The data for the following simulations was generated using homemade codes written in FORTRAN, using different packages, such as LAPACK and OPENBLAS. The algorithm to solve the Master Equation is shown in the Appx C. We considered a wave packet $|\phi\rangle$ initially concentrated in the center of a 1D chain lattice as an initial condition, for most of the simulations, and constructed the density matrix from it. Then, we solved the Master Equation (see Eq. 3.1) with some or all dissipators, according to the property we were analyzing. Finally, we plot the figures with the obtained data using Grace software.

4.1 Spreading of the wave packet

Important information about how the dephasing strength γ_ϕ affects the transport properties of our system can be extracted by observing the propagation of an initially localized wave packet. We considered a wave packet initially concentrated in the center of the chain and solved the Eq. 3.1 with the Haken-Strobl pure dephasing (see Eq. 3.4).

Figure 4.1 shows the behavior of the probability to find an excitation on each site for a wave packet initially concentrated in the center of a chain of $N = 100$ sites at different times and for different values of W/Ω and γ_ϕ.

Figure 4.1 is organized by columns and rows. The left column refers to the case $W/\Omega = 0$; metallic regime. The columns of the middle refer to the case $W/\Omega = 2$; MIT. At last, the right columns refer to the case $W/\Omega = 20$; localized regime. The rows are for different instants of time, with four orders of magnitude difference between them. In all the three regimes, at short times, the probability of finding the excitation in the middle of the lattices is one, and zero in all other sites; see upper panels. Also, we observed that as W/Ω increases, it takes longer for the system to have a homogeneous distribution. Additionally, the probability propagates along the chain until it turns into a homogeneous distribution for $\gamma_\phi > 0$.

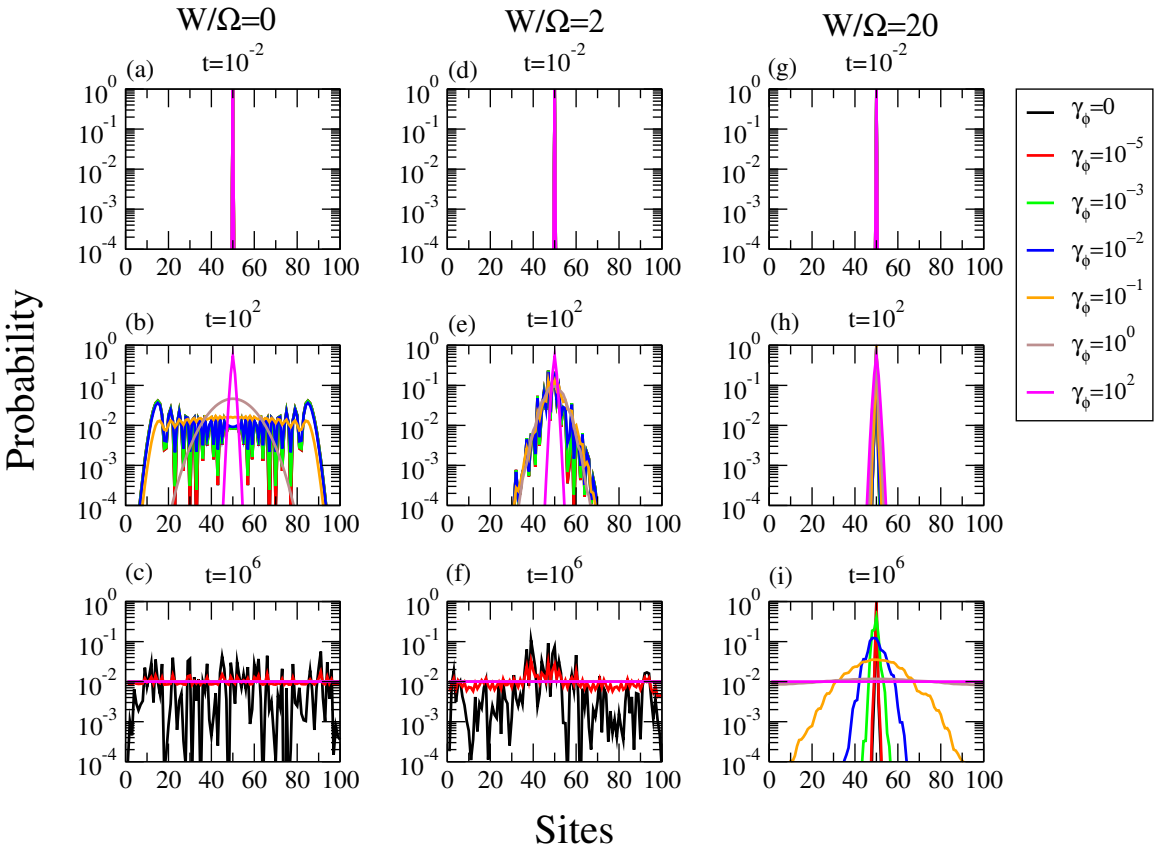

Figure 4.1: The probability of finding an excitation on each site for a wave packet initially concentrated in the center of the chain for different values of γ_ϕ, W/Ω and time. We solve the Master Equation Eq. 3.1 with Haken-Strobl pure dephasing. The figure is organized by columns and rows. Left columns refer to the case $W/\Omega = 0$; regime. Middle columns refer to the case $W/\Omega = 2$; MIT. Right columns refer to the case $W/\Omega = 20$; localized regime. The rows are for different instants of time, with four orders of magnitude difference between them. The parameters in this figure are: $N = 100$, $\Omega = 1cm^{-1}$, $\beta = (\sqrt{5}-1)/2$ and $\hbar = 5.29cm^{-1}ps$.

4.2 Different transport regimes

Here we define the main transport regimes which can be observed in a quantum system:

1) **Ballistic transport.** Ballistic transport describes the motion of a particle or excitation traveling at constant speeds within a medium without scattering and is characterized by a linear spreading of the wave packet, so we have

$$\sigma^2(t) = v^2 t^2 \tag{4.1}$$

where $\sigma^2(t)$ is the variance of an initial localized wave packet, see more detailed definition below.

2) **Diffusive transport.** Diffusive transport describes the motion of a particle or excitation within a medium with scattering and it is characterized by a spreading of the wave packet which depends on the square root of the time, so we have:

$$\sigma^2(t) = 2Dt \tag{4.2}$$

where D is the diffusion coefficient.

For both, ballistic and diffusive transport, the excitation will evenly spread over all the system at long times, until it will have equal probability over all the sites, so at saturation we have $\sigma^2 = \sum_{i=-N/2}^{N/2} i^2/N$, so that

$$\sigma^2_{Sat} = N^2/12. \tag{4.3}$$

3) **Localized transport regime.** In this regime the excitation remains mostly in the initial site and it spreads only up to a certain localization length, which is less than the saturation value of the variance given in Eq. 4.3.

4.3 Diffusion coefficient

In this section, we focus on the diffusion coefficient. In the beginning, we derive the formula for the diffusion coefficient following [41]. Then, we show the typical behavior of the diffusion coefficient for different values of W/Ω, dephasing strength and for different system size.

To compute the diffusion coefficient D, we use the approach used by Jianshu Cao [41], which allows us to compute the diffusion coefficient for the Haken-Strobl model only by diagonalizing the Hamiltonian Eq. 2.1. The diffusion coefficient can be studied in the direction along the unit vector $\mathbf{u}$ using the Green-Kubo expression:

$$D(\mathbf{u}) = \frac{1}{Z_s}\int_0^\infty Tr\left[e^{-\beta H_s} j(\mathbf{u},t) j(\mathbf{u})\right] dt\,, \tag{4.4}$$

where Z_s is the partition function of the system. In the Haken-Strobl approach, we take infinite temperature ($\beta = 0$), so $Z_s = N$. The flux operator $j(\mathbf{u})$ and its time derivative are given by:

$$j(\mathbf{u}) = i\sum_{n,m}(\mathbf{u}\cdot\mathbf{r}_{nm})\Omega_{nm}\left|m\right\rangle\left\langle n\right|\,, \tag{4.5}$$

$$\frac{d}{dt}j(\mathbf{u},t) = i\left[j(\mathbf{u},t), H_s\right] - \frac{\gamma_\phi}{2}\sum_n\left[V_\mathbf{n},\left[V_\mathbf{n}, j(\mathbf{u},t)\right]\right]\,, \tag{4.6}$$

where γ_ϕ is the dephasing ratio, $\mathbf{r}_{m,n}$ is the vector that connects the site m with the site n, $\Omega_{n,m}$ is the nearest neighbor coupling and $V_\mathbf{n} = \left|n\right\rangle\left\langle n\right|$ is a completeness relation in the site base. The solution for Eq. 4.6 in the Heisenberg picture is:

$$j(\mathbf{u},t) = e^{iH_s t} j e^{-iH_s t} e^{\gamma_\phi t}\,. \tag{4.7}$$

By substituting Eq. 4.5 and 4.7 into Eq. 4.4, carrying out the integration over time analytically, and inserting two completeness relations in the system eigenbasis, we obtain:

$$D(\mathbf{u}) = \frac{1}{N}\sum_{\mu,\nu=1}^{N}\frac{\gamma_\phi + i\omega_{\mu,\nu}}{\gamma_\phi^2 + \omega_{\mu,\nu}^2}\left|j_{\mu,\nu}(\mathbf{u})\right|^2\,, \tag{4.8}$$

where $\omega_{\mu,\nu}$ is the difference of the eigenvalues of the system, ϕ_n^ν is the component of the amplitude of the eigenstate ν of the site n and $j_{\mu,\nu}(\mathbf{u})$ is the flux operator in the eigenbasis. The flux operator in the eigenbasis is given by:

$$j_{\nu,\mu}(\mathbf{u}) = i\sum_{n.m}(\mathbf{u}\cdot\mathbf{r}_{n,m})\phi_n^{\mu *}\phi_m^\nu\Omega_{n,m}\,. \tag{4.9}$$

Now, we need to take the real part of Eq. 4.8. For this, we create an analogous equation using the fact that $w_{\mu,\nu} = -w_{\nu,\mu}$,

$$D(\mathbf{u}) = \frac{1}{N}\sum_{\mu,\nu=1}^{N} \frac{\gamma_\phi - i\omega_{\nu,\mu}}{\gamma_\phi^2 + \omega_{\nu,\mu}^2} |j_{\mu,\nu}(\mathbf{u})|^2 \,. \tag{4.10}$$

Finally, we add Eq. 4.8 and Eq. 4.10 to obtain:

$$D(\mathbf{u}) = \frac{1}{N}\sum_{\mu,\nu=1}^{N} \frac{\gamma_\phi}{\gamma_\phi^2 + \omega_{\mu,\nu}^2} |j_{\mu,\nu}(\mathbf{u})|^2 \,. \tag{4.11}$$

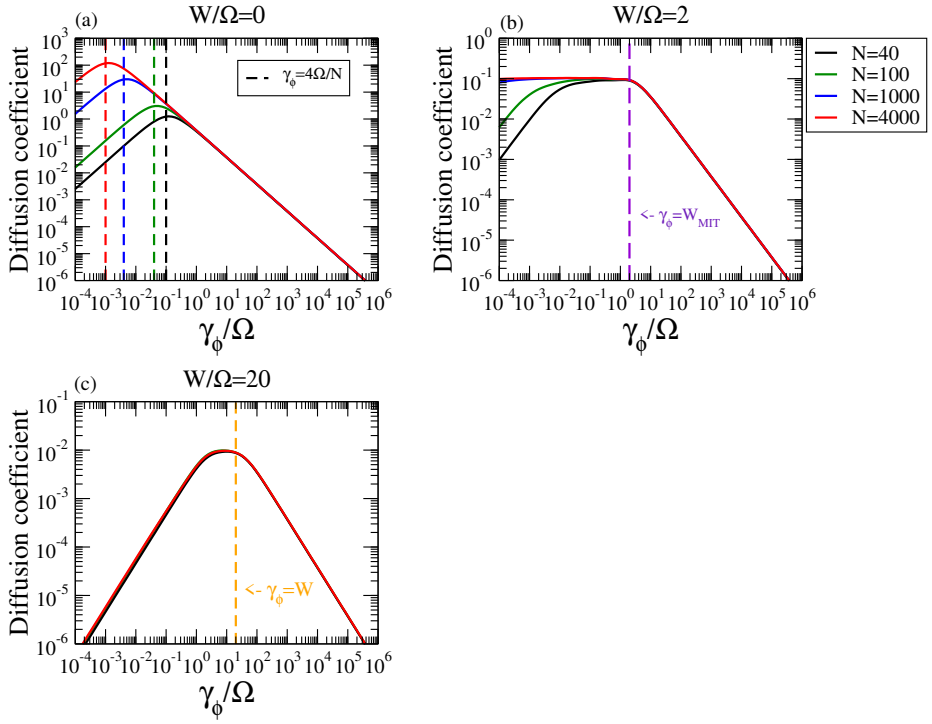

Figure 4.2: Diffusion coefficient as a function of γ_ϕ/Ω for different values of system size and W/Ω. To produce this figure, we use Eq. 4.11. This figure is organized in three different panels; each panel for a different value of W/Ω. Panel (a) is for $W/\Omega = 0$; metallic regime. The vertical dashed lines mark the value when the dephasing starts to become dominant in the transport behavior. This value depends directly on the system size $\gamma_\phi/\Omega = 4/N$. Panel (b) is for the MIT, $W/\Omega = 2$. The vertical dashed line is the critical value $\gamma_\phi/\Omega = W/\Omega = 2$ at which the diffusion coefficient desists to be independent of dephasing and begins to decrease. Panel (c) is for $W/\Omega = 20$; insulating regime. The vertical dashed line is obtained from $\gamma_\phi/\Omega = W/\Omega$ and marks the time when the diffusion coefficient reaches a maximum value. The parameters in this figure are: $\Omega = 1cm^{-1}$, $\beta = (\sqrt{5}-1)/2$ and $\hbar = 5.29cm^{-1}ps$.

Figure 4.2 shows the typical behavior of the diffusion coefficient (see Eq. 4.11) as a function of γ_ϕ/Ω for different values of W/Ω and system size. This figure is organized into three panels; each panel is for a different value of W/Ω. Panel (a) corresponds to

$W/\Omega = 0$; metallic regime. Here, it is seen that for small values of γ_ϕ/Ω, the diffusion coefficient increases with γ_ϕ/Ω up to $\gamma_\phi = 4\Omega/N$ (see the vertical dashed lines), then the diffusion coefficient starts to decay. $4\Omega/N$ is the mean leval spacing in absence of disorder. The value $\gamma_\phi = 4\Omega/N$ refers to the point at which dephasing starts to become dominant in the transport behavior. Thus as the system size increases in the metallic regime, the diffusion coefficient only decreases. Panel (b) corresponds to the MIT. In this panel, we can observe the independence of the diffusion coefficient to dephasing up to a critical value of dephasing $\gamma_\phi = W_{MIT}$ that is independent of the system size (see the vertical magenta dashed line). This effect is more evident as the system size increases due to the reduction of finite size effects. After that critical value of dephasing, the diffusion coefficient begins to decrease. Panel (c) is for $W/\Omega = 20$; insulating regime. Here, it can be seen that the diffusion coefficient reaches a maximum that is independent of the system size. Summarizing, Fig. 4.2 shows that, in the large system size limit, the diffusion coefficient has a particular behavior for each regime. In the metallic regime, the diffusion coefficient always decreases with dephasing. In the insulating regime, the diffusion coefficient reaches a maximum at $\gamma_\phi/\Omega = W/\Omega$. Finally, in the MIT, the diffusion coefficient is independent of γ_ϕ up to a critical value of γ_ϕ and then it decreases. This latest surprising result is one of the main findings of this thesis.

Figure 4.3 shows a direct comparison of the typical behavior of the diffusion coefficient (see Eq. 4.11) as a function of γ_ϕ/Ω for different values of W/Ω for a system size of $N = 10^4$. The domain of this figure starts at $\gamma_\phi/\Omega = 4/N$, so that we disregard finite site effects. Here we notice three behaviors. For values of $W/\Omega < 2$, the diffusion coefficient only decreases. Then, For values of $W/\Omega > 2$, the diffusion coefficient reaches a maximum value. Lastly, for the value of $W/\Omega = 2$, the diffusion coefficient is independent to γ_ϕ up to a critical value of $\gamma_\phi = 2$ as the vertical dashed orange line indicates.

Figure 4.4 shows the behavior of the diffusion coefficient as a function of W/Ω for different dephasing strengths in a system size of $N = 5 \times 10^4$. We focus our attention on the behavior of diffusion coefficient around $W/\Omega = 2$ to show that only at the MIT the diffusion coefficient is independent of dephasing. Figure 4.4 shows one intersection between the different curves at $W/\Omega = 2$ as indicated by the vertical dashed orange line. This intersection confirms that there is a single point through the W/Ω values where the transport is independent of γ_ϕ up to a critical value of γ_ϕ. We have used values of dephasing between the mean level spacing ($\gamma_\phi = 4\Omega/N$) and the critical value of dephasing ($\gamma_\phi = W_{MIT}$) where

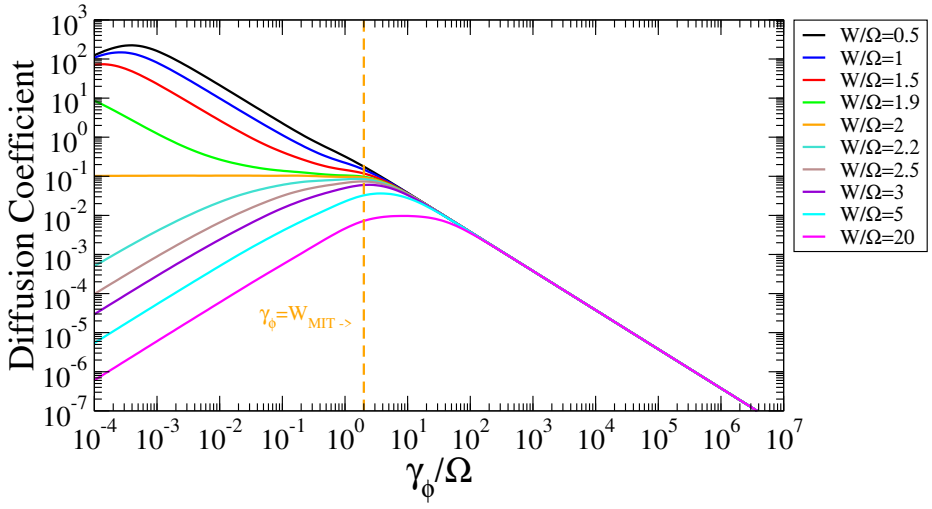

Figure 4.3: Diffusion coefficient as a function of γ_ϕ/Ω for different values of W/Ω in a system size of $N = 10^4$. For this figure, we use the Eq. 4.11. The dashed orange vertical line in the figure corresponds to $\gamma_\phi/\Omega = W/\Omega = 2$ that marks the value when D stops to be independent of dephasing for $W/\Omega = 2$ (orange curve). The parameters in this figure are: $\Omega = 1cm^{-1}$, $\beta = (\sqrt{5}-1)/2$ and $\hbar = 5.29cm^{-1}ps$.

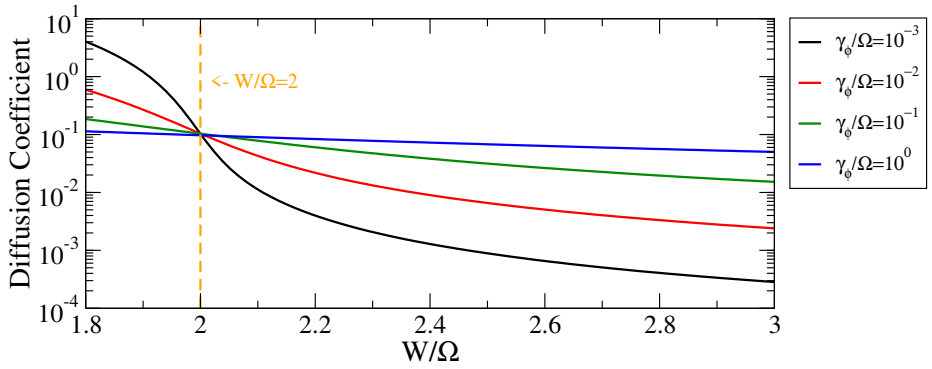

Figure 4.4: Diffusion coefficient as a function of W/Ω for different values of γ_ϕ/Ω in a system size of $N = 5 \times 10^4$. In this figure, we use Eq. 4.11. The dash vertical orange line marks the MIT, where the curves intersect. The parameters in this figure are: $\Omega = 1cm^{-1}$, $\beta = (\sqrt{5}-1)/2$ and $\hbar = 5.29cm^{-1}ps$.

D starts to decrease.

4.4 Dynamics: wave packet spreading

In this section, we center our attention on studying the dynamics of wave packet spreading. We split the section into two subsections. The first subsection is for the spreading of a wave packet in absence of dephasing. First, we obtain an analytical expression for the diffusion coefficient, considering how the motion of the wave packet spreads and computing the time when the motion changes from ballistic to diffusive. Last, we show the spreading of a wave packet for different values of W/Ω using the wave packet variance. The second subsection analyzes the spreading of the wave packet in presence of dephasing. Here, we show how the dynamics changes taking into account different orders of magnitude of the dephasing strength for different values of W/Ω. Finally, we show a comparison between the diffusion coefficient that we obtain using Eq. 4.11 (see previous section Sec. 4.3) and the one obtained from the dynamics given by the Master Equation.

4.4.1 Spreading in absence of dephasing

Given a wave packet $|\psi(t)\rangle$ we can define the variance of spacial probability distribution of the excitation on the chain in the following way:

$$\sigma^2(t) \equiv \langle r^2(t)\rangle - \langle r(t)\rangle^2 \,, \tag{4.12}$$

where

$$\langle r^2(t)\rangle = \sum_{i=1}^{N} i^2 |\, \langle i|\psi(t)\rangle \,|^2 \quad \text{and} \quad \langle r(t)\rangle = \sum_{i=1}^{N} i |\, \langle i|\psi(t)\rangle \,|^2 \,. \tag{4.13}$$

Let us first concentrate on the case of zero dephasing. The variance for ballistic motion is given by

$$\sigma^2(t) = v^2 t^2 \,, \tag{4.14}$$

where the v is the velocity given by

$$v = \sqrt{2} a \frac{\Omega}{\hbar} \,, \tag{4.15}$$

and a is the lattice step, as we verified numerically (not shown). In the diffusive regime, the second moment is

$$\sigma^2(t) = 2Dt \,, \tag{4.16}$$

where D is the diffusion coefficient.

At the beginning of the wave packet, spreading is always ballistic, up to the mean free time $\mathcal{T} = \hbar/W$. The mean free time $\mathcal{T}$ is the time where the spreading changes from ballistic to diffusive. Before the time $\mathcal{T} = \hbar/W$ in Eq. 4.14, the variance spreads in a ballistic way up to the mean free path l squared [42, 43]. Substituting Eq. 4.15 at $\mathcal{T}$ in Eq. 4.14, we obtain the mean free path squared:

$$l^2 = \sigma^2(\mathcal{T}) = v^2\mathcal{T} = 2\left(a\frac{\Omega}{\hbar}\frac{\hbar}{W}\right)^2 = 2\left(\frac{a\Omega}{W}\right)^2 . \tag{4.17}$$

From the latter expression, we have $l = \sqrt{2}a\Omega/W$. If we do this in the MIT, where $W = 2\Omega$, we obtain $l = a/\sqrt{2}$.

Eventually, for Eq. 4.16, we can express D in terms of l and $\mathcal{T}$ as

$$D = \frac{l^2}{2\mathcal{T}} , \tag{4.18}$$

so that we have the analytical expression for the diffusion coefficient at the MIT for zero dephasing. Nevertheless, from numerical simulations (see Fig. 4.5), we note that only at the MIT the motion is truly diffusive since from any $W/\Omega < 2$ the motion returns to be ballistic at sufficiently long times. Using the above expression we have that, at the MIT, the diffusion coefficient is given by

$$D_{MIT} = \frac{a^2\Omega}{2\hbar} . \tag{4.19}$$

This expression is verified to give the correct diffusion coefficient at the MIT in Fig. 4.5.

Figure 4.5 shows the typical behavior of the dynamics of the spreading of a wave packet in absences of dephasing as a function of time for a system size of $N = 10^4$ for different values of W/Ω. To obtain Fig. 4.5, we consider a wave packet initially concentrated in the center of the chain as an initial condition. Then, we solve Eq. 3.1 without dissipators. Finally, we use the variance Eq. 4.12 to study the spreading of the wave packet. We notice that the dynamics of the wave packet for $W/\Omega < 2$ is saturated at large times, and it is obtained using Eq. 4.3. While for $W/\Omega > 2$ at longer times, the motion is localized and has a value much less than the saturation value. In particular, for $W/\Omega = 0$, the dynamics is purely ballistic, but for values of $0 < W/\Omega < 2$, the motion goes from ballistic to diffusive for a short period of time and then returns to ballistic. When the dynamics of the system is ballistic, it can be fit using Eq. 4.14 times a constant c. Where the constant for $W/\Omega = 0$,

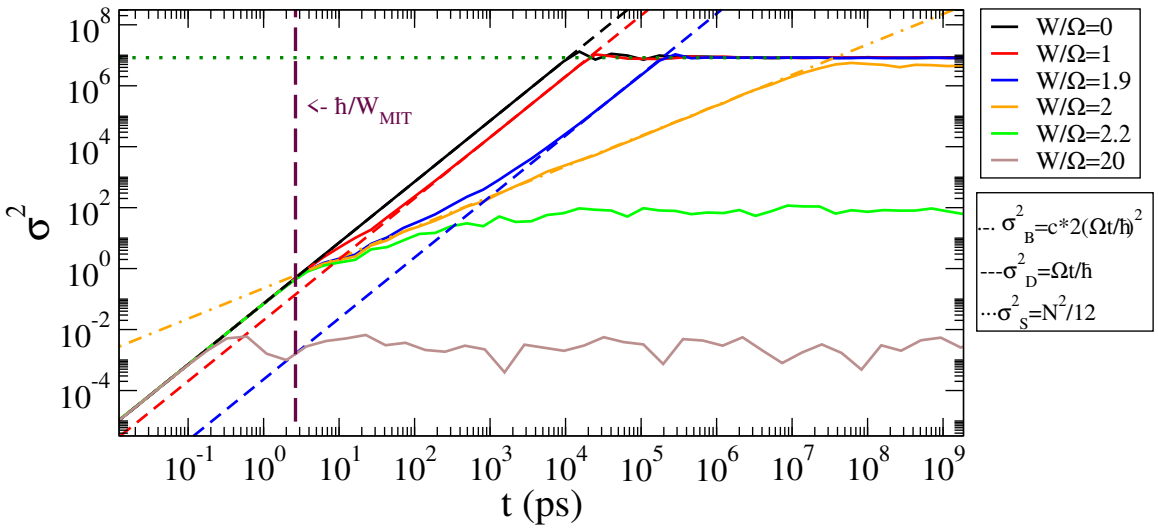

Figure 4.5: Dynamics of the spreading of a wave packet initially concentrated in the center of the chain. The wave packet variance Eq. 4.12 is shown in absence of dephasing, as a function of time for a system size of $N = 10^4$ and for different values of W/Ω. For values of $W/\Omega < 2$; metallic regime, the dynamics at large times is always ballistic and it can be fit using $\sigma^2 = (\sqrt{2}\Omega t/\hbar)^2 \times c$ (oblique dashed lines). The constants are $c = 1$, $c = 2/7$, and $c = 1/316$ for the black, red, and blue oblique dashed lines, respectively. The horizontal green dotted line shows the equilibrium value of the variance for $W/\Omega = 0$ Eq. 4.3. For the MIT $W/\Omega = 2$, the dynamics start as ballistic and then it becomes diffusive. It can be fit with Eq. 4.16 (oblique dash-dotted line). Note that the time in which the dynamics changes from ballistic to diffusive is $\hbar/W$, see vertical dashed line. For $W/\Omega > 2$, insulating regime, the dynamics start as ballistic and then it reaches an equilibrium value much smaller than the value reached in $W/\Omega = 0$. The variance is normalized to the lattice step so that σ^2 really means σ^2/a^2. The parameters in this figure are: $\beta = (\sqrt{5}-1)/2$, $\Omega = 1cm^{-1}$, $N = 10^4$, and $\hbar = 5.29cm^{-1}ps$.

$W/\Omega = 1$, and $W/\Omega = 1.9$ is $c = 1$, $c = 2/7$, and $c = 1/316$, respectively. Moreover, we find that when $W/\Omega = 2$ the dynamics pass from being ballistic to be, purely diffusive. We use Eq. 4.16 using the D of Eq. 4.19 to describe the diffusive motion of the wave packet. Finally, when $W/\Omega > 2$, the motion starts as ballistic and becomes localized quickly.

4.4.2 Spreading in presences of dephasing

Figure. 4.6, we study the dynamics of the wave packet spreading in the presence of dephasing. To obtain the Fig. 4.6, we consider a wave packet initially concentrated in the center of the chain as an initial condition. Then, we solve Eq. 3.1 with the Haken-Strobl pure dephasing (see Eq. 3.4). Finally, we use the variance Eq. 4.12 to study the dynamics of the spreading of the wave packet. This figure shows different panels of the dynamics of the wave packet propagation as a function of time considering different orders of magnitude of γ_ϕ/Ω in a system of size $N = 100$; each panel is for a different value of W/Ω. Panel (a) corresponds to $W/\Omega = 0$; metallic regime. Here, we notice that independently of the value of dephasing, all the motions always begin ballistically. In general, when $\gamma_\phi/\Omega > 0$, the motion changes the behavior from ballistic to diffusive. The time where the dynamics changes from ballistic to diffusive is $t = \hbar/\gamma_\phi$ (see the continuous vertical line). Panel (b) corresponds to the MIT; $W/\Omega = 2$. As seen in the latter panel, the motion starts ballistically and then changes from ballistic to diffusive after a specific time. Here, the time required to change the type of motion is the smaller time between $\hbar/W$ (see the dashed vertical line) and $\hbar/\gamma_\phi$ (see the continuous vertical lines). Interestingly, the transport is independent of γ_ϕ up to a critical value $\gamma_\phi = W_{MIT}$. Panel (c) is for $W/\Omega = 20$; insulating regime. Here, the motion of the wave packet spreading starts ballistic independently of the dephasing value. We notice that if $W/\Omega > \gamma_\phi/\Omega$, the motion remains localized for a little time-lapse and then changes to diffusive. While if $\gamma_\phi/\Omega \geq W/\Omega$ the motion changes from ballistic to diffusive directly. Furthermore, the time where the diffusive motion starts is $\hbar/\gamma_\phi$. In summary, for all the panels, to model the diffusive motion, we use Eq. 4.16, where the diffusion coefficient D is obtained from Eq. 4.11 (see the oblique dashed lines). In particular, we notice that in the localized regime D given by Eq. 4.11 does not always work.

Figure 4.7 shows the diffusion coefficient as a function of γ_ϕ/Ω for different values of W/Ω in a system size of $N = 100$. The main objective of this figure is to show until which

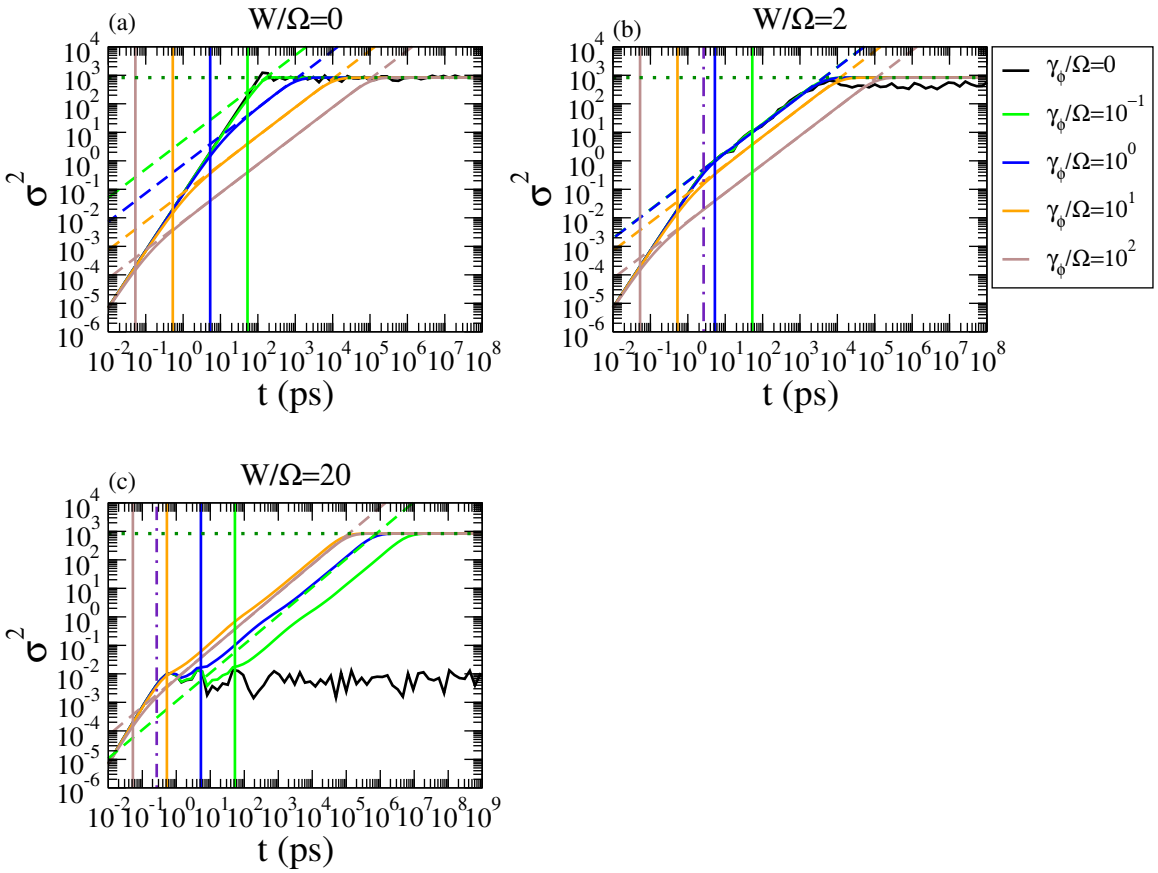

Figure 4.6: Dynamics of the spreading of a wave packet initially concentrated in the central site of the chain, for different values of W/Ω and γ_ϕ/Ω. To produce this figure, we solve the Master Equation Eq. 3.1 with the Haken-Strobl pure dephasing Eq. 3.4 and use the Eq. 4.12. This figure is organized into three panels; each panel is for a different value of W/Ω. Panel (a) is for $W/\Omega = 0$; metallic regime. Here, the time where the dynamics changes from ballistic to diffusive is $t = \hbar/\gamma_\phi$ (see the continuous vertical lines). Panel (b) is for the MIT; $W/\Omega = 2$. Here, the time required to change the type of motion is the smallest time between $\hbar/W$ (see the dashed vertical line) and $\hbar/\gamma_\phi$ (see the continuous vertical lines). Panel (c) is for $W/\Omega = 20$; insulating regime. Here, the time where the diffusive motion starts is $\hbar/\gamma_\phi$. The value equilibrium value $\sigma_{sat} = N^2/12$ is indicated as a horizontal green dashed line in all panels. Also, in all panels, the oblique dashed lines correspond to a diffusive motion $\sigma^2 = 2Dt$ (Eq. 4.16), where the diffusion coefficient has been obtained from Eq. 4.11. Note that in the insulating regime and $W > \gamma_\phi$, Eq. 4.11 does not work (see the dashed oblique green line). The variance is normalized to the lattice step, so that σ^2 really means σ^2/a^2. The parameters in this figure are: $N = 100$, $\Omega = 1cm^{-1}$, $\beta = (\sqrt{5}-1)/2$, and $\hbar = 5.29cm^{-1}ps$.

value of dephasing the diffusion coefficient D obtained using Eq. 4.11 is accurate. For this,

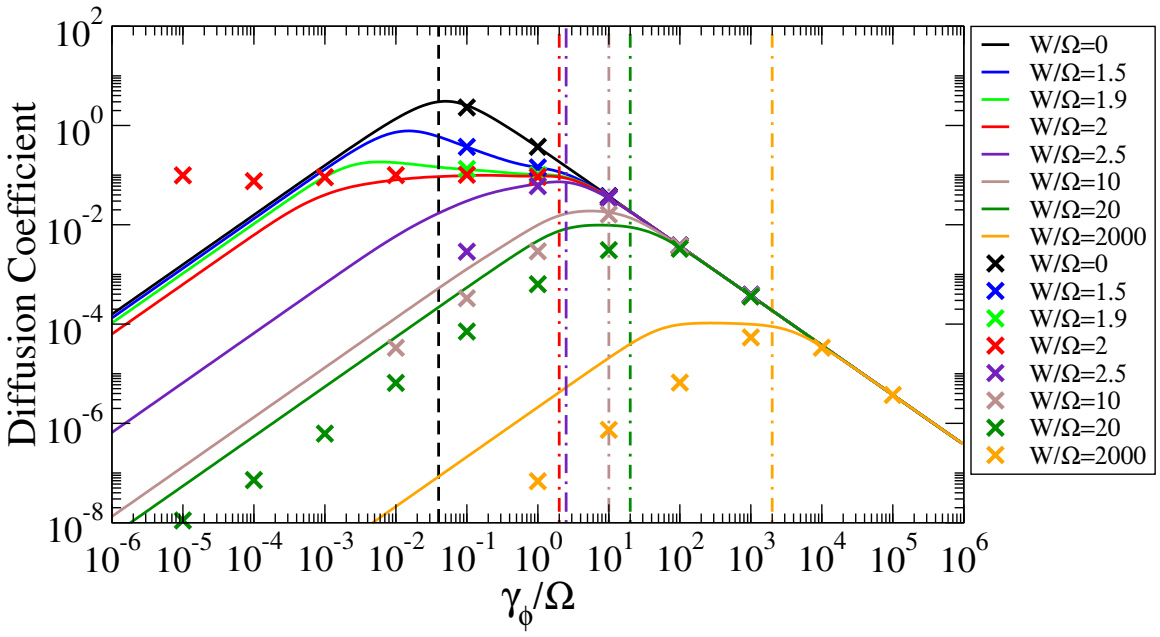

Figure 4.7: Diffusion coefficient as a function of γ_ϕ/Ω for different values of W/Ω in a system size of $N = 10^2$. In this figure, we compare the diffusion coefficient given by Eq. 3.1 (see the symbols) and given by Eq. 4.11 (see the continues curves). The vertical dashed black line marks when $\gamma_\phi = 4\Omega/N$. The vertical dash-dotted line marks when $\gamma_\phi = W$. The parameters are: $\Omega = 1cm^{-1cm}$, $\beta = (\sqrt{5}-1)/2$ and $\hbar = 5.29cm^{-1}ps$.

we compare D obtained for the Eq. 3.1 (symbols) against the Eq. 4.11 (continuous curves). To obtain D from the Master Equation method, we fit the linear part of the variance of the spreading wave packet from the Fig. 4.6 as $y = a_1 x + a_0$, where $D = a_1/2$. In the metallic regime crosses are not shown for values of the dephasing strengths for which the motion is not diffusive. When the motion is diffusive, we can see that the values of D obtained with both methods are in agreement. This occurs for $\gamma_\phi > 4\Omega/N$ (see the black dashed vertical line). Note that at the MIT and for $\gamma_\phi < 4\Omega/N$ the diffusion coefficient obtained from Eq. 4.11 does not work even if the motion is diffusive. Work is in progress to understand this discrepancies. Finally we also note that the diffusion coefficient obtained from Eq. 4.11 overestimates the diffusion coefficient obtained dynamically for small dephaisng strength $\gamma_\phi < W$. Also in this case work is in progress to understand this deviations. Overall the analysis presented in this figure qualitatively confirms the conclusions of the previous section. In Appx D, we show the corresponding dynamics of the wave packet in presence of dephasing which we used to produce the data shown in Fig. 4.7.

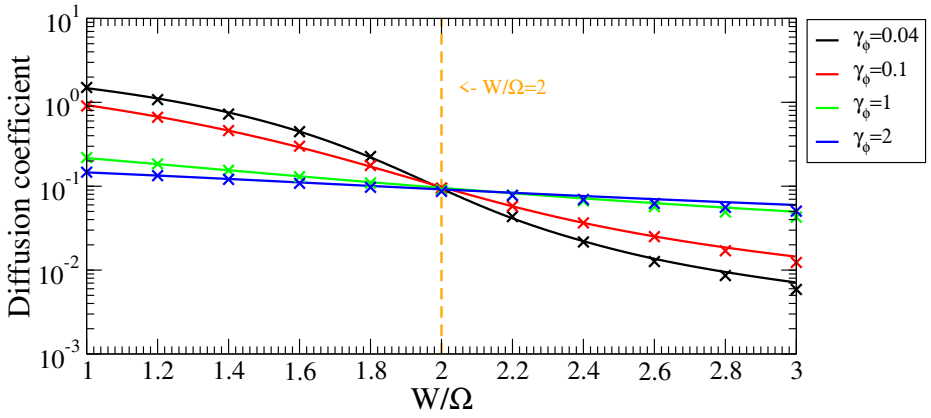

Figure 4.8: Diffusion coefficient as a function of W/Ω for different values of γ_ϕ/Ω in a system size of $N = 10^2$. In this figure, we compare the diffusion coefficient given by Eq. 3.1 (see the symbols) and given by Eq. 4.11 (see the continues curves). The dash vertical orange line marks the MIT, where the curves intersect with each other. The parameters in this figure are: $\Omega = 1cm^{-1}$, $\beta = (\sqrt{5}-1)/2$ and $\hbar = 5.29cm^{-1}ps$.

Figure 4.8, we compare the D given by Eq. 3.1 (see the symbols) with the given by Eq. 4.11 (see the continues curves) as a function of W/Ω for different values of dephasing. Note that this figure is similar to Fig 4.3 but with a smaller value of N, indeed here $N = 10^2$. This is due to the numerical limitations of using the Master Equation method for long chains. In this figure dephainsg strengths in the range $4\Omega/N \leq \gamma_\phi \leq 2\Omega$ are shown. Whithin this range perfect agreement can be seen between the diffusion coefficints computed with the two different methods.

4.5 Stationary steady-state current

The last property we study is the stationary steady-state current I_{ss}. The steady-state current here means the time independent value that the current reaches after a transient time. We use four methods to study I_{ss}. In the first subsection, we use the Master Equation 3.1 to obtain I_{ss}. In the second subsection, we obtain I_{ss} using the average transfer time in absence of dephasing and compare this method with the Master Equation. In the third subsection, we obtain I_{ss} using the average transfer time in presences of dephasing and compare this method with the Master Equation. In the fourth subsection, we make a heuristic construction of the mean transfer time using the diffusion coefficient. Then, we make a comparison between all the methods of this section. Last, we show the typical

behavior of I_{ss} as a function of dephasing for different values of W/Ω for a larger system size.

4.5.1 Master Equation

From the steady-state solution of Eq. 3.9, we can find the stationary steady-state current

$$I_{ss} = \frac{\gamma_d}{\hbar} \langle N| \rho_{ss} |N\rangle \ , \tag{4.20}$$

where ρ_{ss} is the steady-state density operator [25].

Figure 4.9 shows different panels of the typical behavior of the steady-state current as a function of γ_ϕ/Ω for different values of W/Ω and system size; each panel is for a different value of W/Ω. We use Eq. 4.20 to generate the figure. Panel (a) corresponds to $W/\Omega = 0$; metallic regime. This panel shows that the steady-state current decreases with dephainsg for $\gamma_\phi > 4\Omega/N$ (see the vertical dashed lines). This implies that in the large system size limit, the current always decreases with dephasing in the metallic regime. Panel (b) corresponds to the MIT; $W/\Omega = 2$. This panel shows that I_{ss} tends to become independent of dephasing for $\gamma_\phi < W$ (see vertical dashed violet line) for large N, see also discussion below. Panel (c) is for $W/\Omega = 20$, insulating regime. In this panel, the current reaches a maximum value independent of the system size (see vertical dashed violet line). Summarizing Fig. 4.9, it shows that in the large system size limit, the I_{ss} has a particular behavior for each regime. In the metallic regime, I_{ss} always decreases with dephasing. In the insulating regime, the I_{ss} reaches a maximum at $\gamma_\phi = W$. Finally, in the MIT, the I_{ss} is independent of the γ_ϕ up to a critical value of γ_ϕ independent of N and then it decreases.

Figure 4.10 shows a direct comparison for the three regimes when the system size is $N = 100$. Here, we highlight that the independence of the current only appears in the MIT up to a critical value of γ_ϕ. The current only decreases with dephasing in the metallic regime, while the current has a maximum value in the insulating regime.

4.5.2 Average Transfer Time in absence of dephasing

In this subsection, we use the Average Transfer Time method to compute the current [25]. This method is computationally less expensive and helps to confirm our previous results on the steady-state current in absence of dephasing.

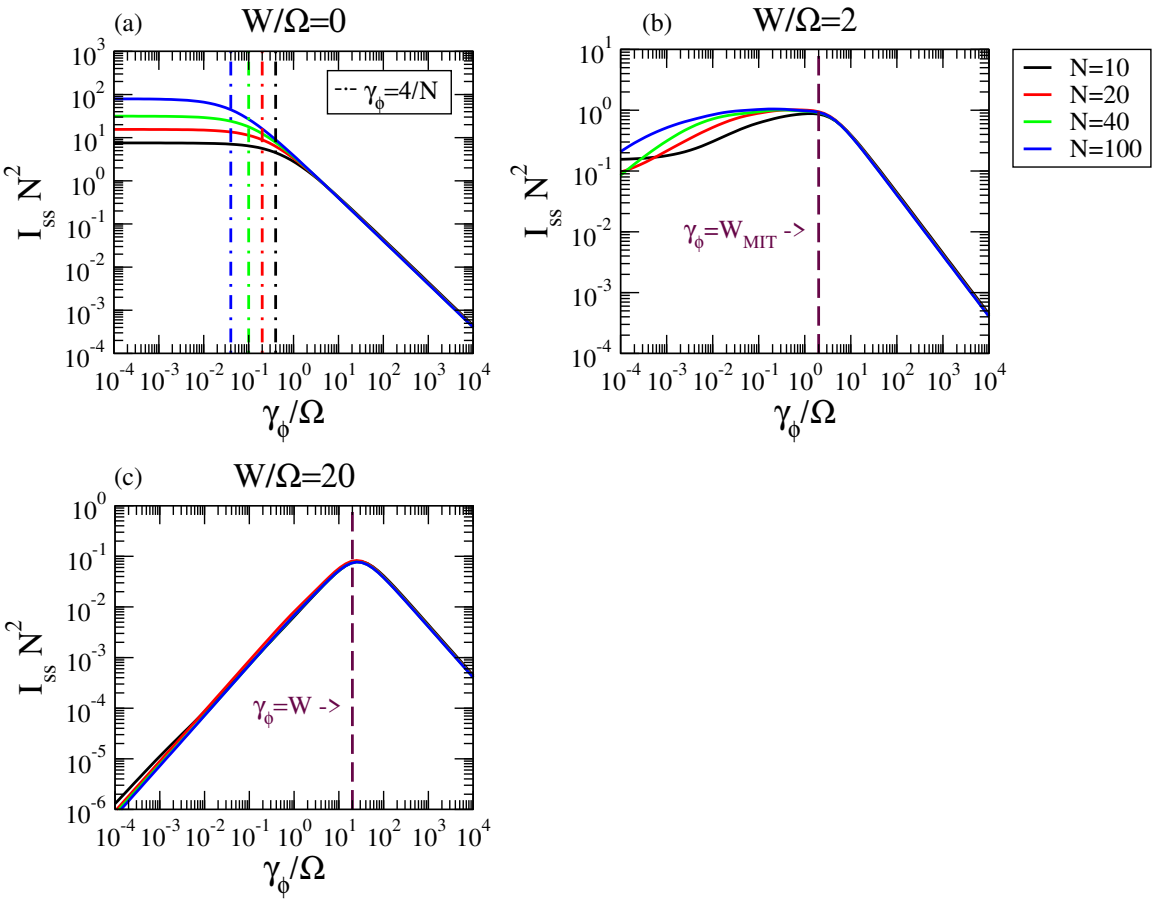

Figure 4.9: Steady-state current as a function of γ_ϕ/Ω for different values of N and W/Ω. To produce this figure, we solve the master equation Eq. 3.1 with Haken-Strobl pure dephasing Eq. 3.4, pumping Eq. 3.7, and draining Eq. 3.8 dissipators. This figure is organized into three panels; each panel is for a different value of W/Ω. Panel(a) is for $W/\Omega = 0$; metallic regime. The vertical dashed lines in this panel mark when $\gamma_\phi/\Omega = 4/N$. Panel (b) is for the MIT; $W/\Omega = 2$. The vertical dashed line is the critical value $\gamma_\phi/\Omega = 2$ when the current starts to decrease. Panel (c) is for $W/\Omega = 20$. The vertical dashed line is the value of $\gamma_\phi = W$ where the current reaches the maximum value. The parameters are: $\Omega = 1cm^{-1cm}$, $\beta = (\sqrt{5}-1)/2$ and $\hbar = 5.29cm^{-1}ps$.

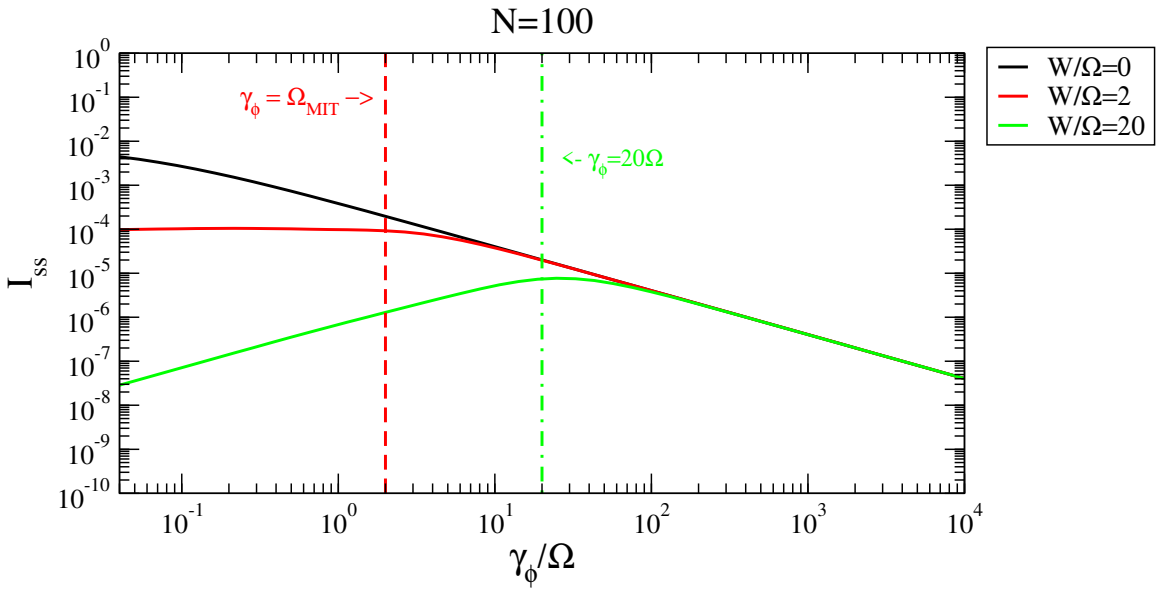

Figure 4.10: Steady-state current as a function of γ_ϕ/Ω for different values of W/Ω for a system size of $N = 100$. This figure shows a direct comparison of the three regimes that are presented in Fig. 4.9. We neglect the finite size effect by showing only the values of the current for $\gamma_\phi > 4\Omega/N$. The vertical dashed line marks $\gamma_\phi/\Omega = 2$. The vertical dash-dotted line marks $\gamma_\phi = W$. The parameters are: $\Omega = 1cm^{-1cm}$, $\beta = (\sqrt{5}-1)/2$ and $\hbar = 5.29cm^{-1}ps$.

To define the current, we compute the average time needed to leave the 1D chain if the excitation is initially on the first site $|1\rangle$ and a drain is present on the last site $|N\rangle$. The average transfer time τ is defined as [25]

$$\tau = \frac{\gamma_d}{\hbar} \int_0^\infty t|\Psi_N(t)|^2 dt\,, \tag{4.21}$$

with $\Psi_N(t) = \langle N| e^{-iH_{eff}t/\hbar} |1\rangle$ being the probability amplitude on the drain site at time t, evolved under the effective Hamiltonian H_{eff}

$$(H_{eff})_{k,l} = (H)_{kl} - i\frac{\gamma_d}{2}\delta_{k,N}\delta_{l,N}\,, \tag{4.22}$$

where H given by Eq. (2.1). The integral in Eq. (4.21) can be evaluated analytically by expanding on the eigenbasis of H_{eff},

$$\tau = \frac{\gamma_d}{\hbar} \int_0^\infty t\,\langle N|e^{-iH_{eff}t/\hbar}|1\rangle\,\langle 1|e^{iH_{eff}t/\hbar}|N\rangle\,dt \tag{4.23}$$

which, being non-Hermitian, has right and left eigenvectors,

$$H_{eff}\,|r_k\rangle = \epsilon_k\,|r_k\rangle \qquad \text{and} \qquad \langle \widetilde{r}_k|\,H_{eff} = \langle \widetilde{r}_k|\,\epsilon_k\,. \tag{4.24}$$

Adding two completeness relation in the base of H_{eff}, then applying H_{eff} over the eigenvector, we obtain:

$$\tau = \frac{\gamma_d}{\hbar} \sum_{k,k'} \langle N|r_k\rangle\,\langle r_k|1\rangle\,\langle N|r_{k'}\rangle^*\,\langle r_{k'}|1\rangle^* \int_0^\infty t e^{-i(\epsilon_k - \epsilon^*_{k'})t/\hbar} dt\,. \tag{4.25}$$

The average transfer time τ is therefore:

$$\tau = \hbar\gamma_d \sum_{k,k'} \frac{\langle N|r_k\rangle\,\langle r_k|1\rangle\,\langle N|r_{k'}\rangle^*\,\langle r_{k'}|1\rangle^*}{-(\epsilon_k - \epsilon^*_{k'})^2}\,, \tag{4.26}$$

and it depends only on the eigenvalues and eigenvectors of H_{eff}.

A rate equation can be derived by assigning a drain frequency $1/\tau$ and a pumping frequency $\gamma_p/\hbar$, connecting the chain population P_e to the vacuum state $|0\rangle$ with population P_0,

$$\begin{aligned} &\frac{dP_0}{dt} = -\frac{\gamma_p}{\hbar}P_0 + \frac{1}{\tau}P_e \\ &P_0 + P_e = 1. \end{aligned} \tag{4.27}$$

From the steady-state population $P_e^{ss} = \gamma_p/(\gamma_p + \frac{\hbar}{\tau})$ we obtain the steady-state current

$$I_{ss} = \frac{P_e^{ss}}{\tau}\,. \tag{4.28}$$

Figure 4.11 shows the steady-state current as a function of W/Ω for different system size obtained with both approaches: the Master Equation approach (ME) Eq. 3.1 and the Average Transfer Time method (ATT) Eq. 4.28. The results obtained with the ATT Eq. 4.28 are identical to the previous ones obtained by the Master Equation Eq. 3.1 as it was proved analytically in [25].

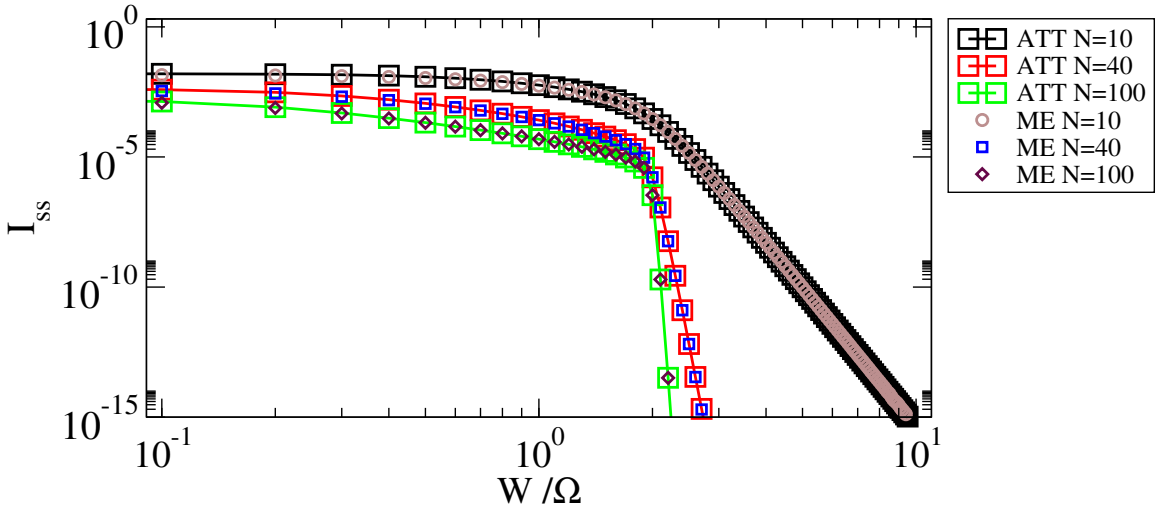

Figure 4.11: Steady-State current as a function of W/Ω for different values of system size in the absence of dephasing. The legends ME and ATT refer to the Master Equation method and Average Transfer Time method, respectively. The parameters are: $W = 2cm^{-1}$, $\Omega = 1cm^{-1}$, $\beta = (\sqrt{5}-1)/2$ and $\hbar = 5.29cm^{-1}ps$.

4.5.3 Average Transfer Time in presences of dephasing

The current computed with the average transfer time in absence of dephasing was proven to be exact in Ref. [25]. Now, in this subsection, we extend the Average Transfer Time method in presence of depahsing to obtain the current. The average transfer time in presence of dephasing can be computed as:

$$\tau_\phi = \frac{\gamma_d}{\hbar}\int_0^\infty t\rho_{NN}(t)dt\,, \tag{4.29}$$

where using the Master Equation Eq. 3.2 in terms of the Liouville superoperator $\mathcal{L}$

$$\dot{\rho}(t) = -\mathcal{L}\rho(t)\,, \tag{4.30}$$

where $\mathcal{L}$ takes into account the Haken-Strobl pure dephasing and draining dissipator, but it does not contain the pumping. Solving Eq. 4.30, we obtain

$$\rho(t) = e^{-\mathcal{L}t}\rho(0)\,. \tag{4.31}$$

Substituting Eq. 4.31 in Eq. 4.29, it gives

$$\tau_\phi = \frac{\gamma_d}{\hbar}\int_0^\infty t\left[e^{-\mathcal{L}t}\rho(0)\right]_{NN} dt\,. \tag{4.32}$$

The average transfer time is therefore

$$\tau_\phi = \frac{\gamma_d}{\hbar}[\mathcal{L}^{-2}\rho(0)]_{NN}\,. \tag{4.33}$$

Finally, similarly to Eq. 4.28, we obtain the steady-state current in the presence of γ_ϕ using the average transfer time:

$$I_{ss} = \frac{P_e^{ss}}{\tau_\phi} \quad \text{with} \quad P_e^{ss} = \frac{\gamma_p}{\gamma_p + \frac{\hbar}{\tau_\phi}}. \tag{4.34}$$

Figure 4.12 shows the comparison of the steady-state current as a function of γ/Ω at MIT for different chain sizes between the results obtained by the Master Equation (ME) Eq. 3.1 and the Average Transfer Time method (ATT) Eq. 4.28. The results obtained with this method are in excellent agreement with the Master Equation approach, even if we do not have a rigorous proof of the equivalence between the two methods as we have in absence of dephasing. Note that the average time method has the advantage of inverting the Liouvillian operator is computationally less expensive than diagonalizing it.

4.5.4 Heuristic Method

Here, we heuristically construct the mean transfer time obtained in the previous section. For the mean transfer time, we consider the draining time and the diffusion time along a chain of N sites. The drain time gives us the time for the excitation to pass from the last site in the chain to $|0\rangle$, while the diffusion time tells us the time for the excitation to go through the entire network.

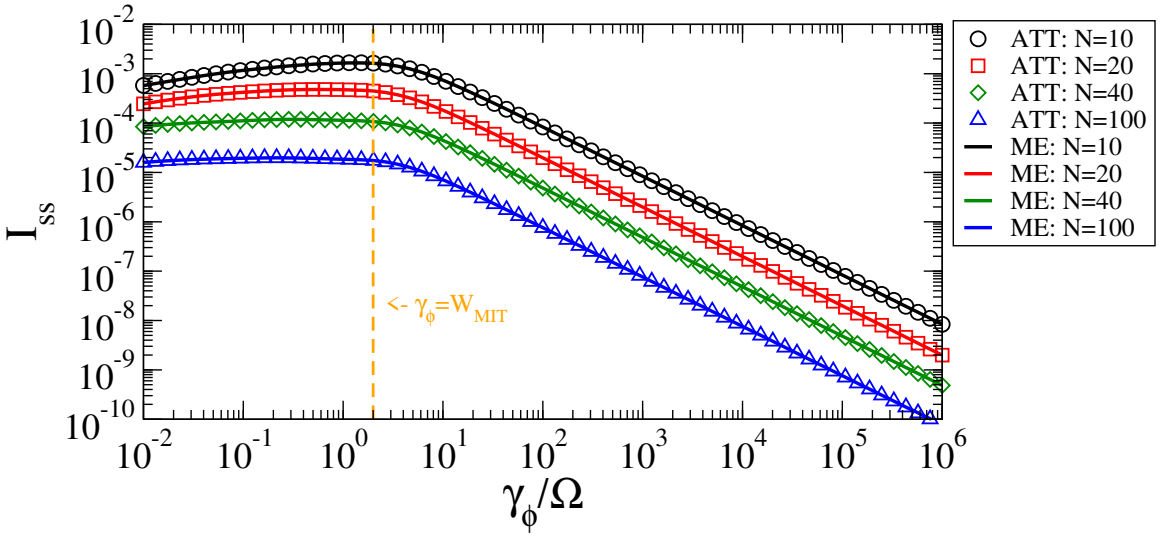

Figure 4.12: Steady-State current as a function of γ_ϕ for different system size at the MIT $W/\Omega = 2$. The legends ME and ATT refer to the Master Equation method Eq. 3.1 and Average Transfer Time method Eq. 4.28, respectively. The vertical dashed line marks the critical value of $\gamma_\phi = W$ where the transport is no longer independent and starts to decrease. The parameters are: $W = 2cm^{-1}$, $\Omega = 1cm^{-1}$, $\beta = (\sqrt{5}-1)/2$ and $\hbar = 5.29cm^{-1}ps$.

To calculate the average transfer time, we start with the drain time. Since at equilibrium the probability of being at site N is $1/N$ and the drain rate is $\gamma_d/\hbar$, we can estimate the drainage time as $\hbar N/\gamma_d$. In order to determine the diffusion time, we know that the time that an excitation takes to go from one site to another is $a^2/(2D)$. Furthermore, we notice that the excitation moves as a random walk and the total number of steps required to perform the random walk in 1D is $N(N-1)$. Then, we can estimate the diffusion time as $N(N-1)a^2/(2D)$ [42]. Thus, adding the drain time and the diffusion time we have

$$\tau_\phi = \hbar\frac{N}{\gamma_d} + \frac{(N-1)N}{2D}a^2\,. \tag{4.35}$$

We can improve this formula cosidering the initial ballistic spreading, so that

$$\tau_\phi = \hbar\frac{N}{\gamma_d} + \tau_{diff} + \tau_{ball}\,. \tag{4.36}$$

To obtain the ballistic time, we remember that the motion is ballistic up to $\hbar/W$, and then the motion becomes diffusive, consequently

$$\tau_{ball} = \hbar/W\,. \tag{4.37}$$

To obtain the diffusive time, we have to subtract the distance traveled in a ballistic motion from the total lattice length $\tilde{N} = aN - l$, hence

$$\tau_{diff} = \frac{\tilde{N}(\tilde{N} - a)}{2D} \,. \tag{4.38}$$

Substituting Eq.4.37 and Eq. 4.38 in Eq. 4.36, we obtain

$$\tau_{\phi} = \hbar \frac{N}{\gamma_d} + \frac{\tilde{N}(\tilde{N} - a)}{2D} + \frac{\hbar}{W} \,. \tag{4.39}$$

For the next figures, when we use the heuristic formula, we obtain D using the Eq. 4.11.

Figure 4.13, we plot the steady-state current as a function of γ_ϕ/Ω at the MIT for a system size of $N = 100$. We use different methods to obtain the I_{ss}; the ME Eq. 3.1, the ATT in presences of dephasing Eq. 4.34, the heuristic equation (HN) Eq. 4.35, and the heuristic equation dividing the diffusive and ballistic time (H$\tilde{\text{N}}$) Eq. 4.39. The results obtained with these approximations are in excellent agreement, except for values of $\gamma_\phi < 4\Omega/N$, since the $\mathcal{D}$ of Eq. 4.11 does not work well for small values of γ_ϕ [44]. The dashed horizontal line is the value of the I_{ss} where is independent of γ_ϕ/Ω. For this line, we use Eq. 4.39 with D_{MIT}.

Figure 4.14, we show the behavior of the I_{ss} as a function of γ_ϕ/Ω for a system size of $N = 10^4$ for different values of W/Ω. We use Eq. 4.39, where the diffusion coefficient is obtained from Eq. 4.11. Here only notice three behaviors. For $W/\Omega < 2$, the I_{ss} only decrease. Then, for values of $W/\Omega > 2$, the I_{ss} only reaches a maximum value. Last, for the value $W/\Omega = 2$, the I_{ss} is independent to γ_ϕ/Ω up to a critical value of $\gamma_\phi/\Omega = 2$ as the vertical dashed orange line indicates. The dashed horizontal line is the value of the I_{ss} when the transport is independent of dephasing. We use Eq. 4.39 with D_{MIT} (see Eq. 4.19).

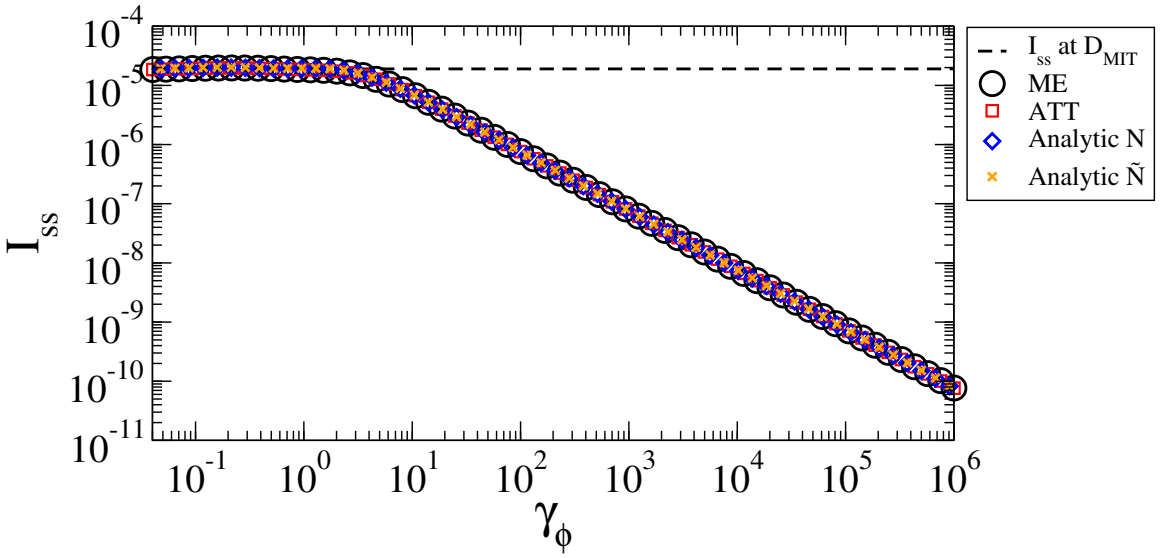

Figure 4.13: Steady-State current as a function of γ_ϕ at the MIT ($W/\Omega = 2$). The legends ME, ATT, HN, and HÑ refer to the Master Equation (Eq. 3.1), Average Transfer Time method (Eq. 4.29), the heuristic equation (Eq. 4.35), and the heuristic equation improved by dividing the diffusive and ballistic time (Eq. 4.39), respectively. The horizontal dashed black line marks the value that the steady-state current takes when it is independent of the dephasing. We obtain this value using Eq. 4.39 where D is from Eq. 4.19. The parameters are: $W = 2cm^{-1}$, $\Omega = 1cm^{-1}$, $\beta = (\sqrt{5}-1)/2$, $N = 100$, and $\hbar = 5.29cm^{-1}ps$.

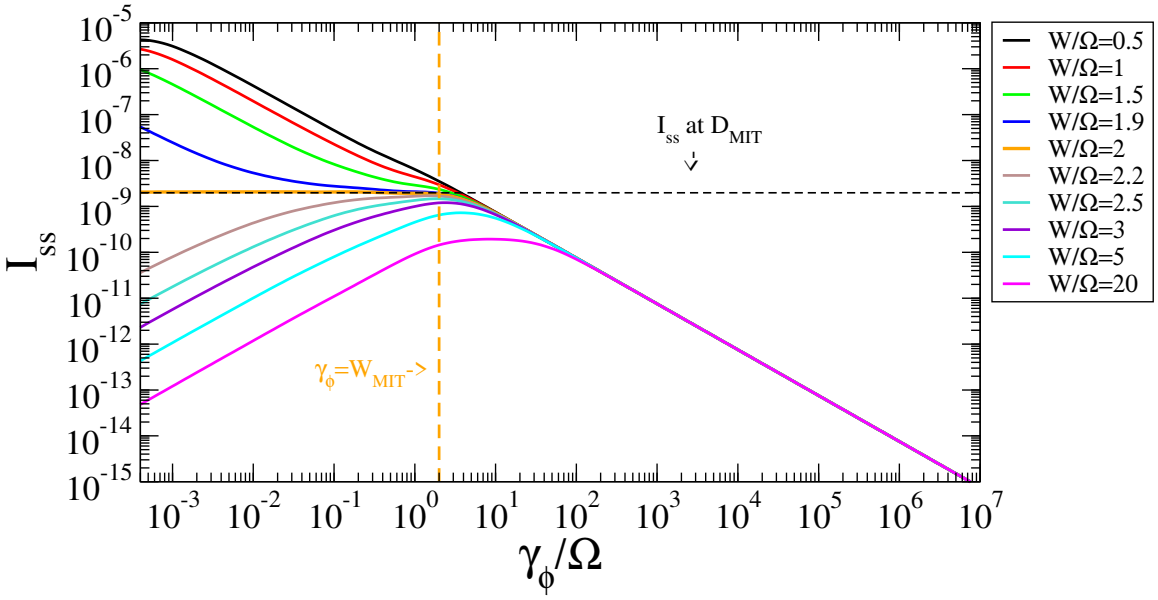

Figure 4.14: Steady-state current as function of γ_ϕ for different values of W/Ω for a system size of $N = 10^4$. For these curves, we use Eq. 4.39, where the diffusion coefficient is obtained from Eq. 4.11. We neglect the finite size effect by showing only the values of the current for $\gamma_\phi > 4\Omega/N$. The vertical dashed orange line represents the critical value of $\gamma_\phi = 2$ where the independence of the current to γ_ϕ/Ω at MIT starts to decrease. The horizontal dashed black line is the value of the steady-state current using the Eq. 4.39, where D is taken from Eq. 4.19. The parameters are: $\Omega = 1cm^{-1}$, $\beta = (\sqrt{5}-1)/2$ and $\hbar = 5.29cm^{-1}ps$.

Chapter 5

Conclusions and perspectives

5.1 Conclusions

In this thesis, we have studied transport in the Harper model in the presence of thermal noise. This model describes the motion of a particle or excitation in a 1D lattice of N sites in the tight-binding approximation, where the site energies are quasi-periodic. The Harper model is interesting since it has a metal-insulator transition in 1D, similar to the 3D Anderson model. This feature has allowed us to study the metal-insulator transition in much larger systems of low dimensionality. Our analysis was inspired by previous literature [26] that claimed that transport was optimal at the MIT. Indeed, transport efficiency is very large in the metallic regime, but dephasing acts very fast in this regime. On the other side, dephasing is very slow in the localized regime while transport efficiency is very low. In [26] it was suggested that the MIT could be an optimal transport regime since transport efficiency is not as bad as in the localized regime, while dephaisng is not as fast as in the metallic regime.

To study the transport properties in the presence of dephasing in the Harper model we have used different figures of merit. By studying the spreading of a wave packet initially localized at the center of the chain, we have shown that at the MIT, the variance evolves in time independently of dephasing up to a critical value of dephasing, $\gamma_\phi = W_{MIT} = 2\Omega$. This critical value does not depend on the system size. We have computed analytically the diffusion coefficient at the MIT: $D_{MIT} = a^2\Omega/2\hbar$. Next, we have studied the steady-state current: we found that also the steady-state current is independent of dephasing up to a critical value of dephasing, $\gamma_\phi = W_{MIT} = 2$, independent of the system size. In order

to study larger system sizes, a different method to compute the steady-state current was developed. This method, based on the computation of the mean transfer time, only requires the inversion of the Liouviliand operator and not its diagonalization. Although we have not given exact proof, we have shown that the results of the steady-state current calculated by the average transfer time method in the presence of dephasing are in perfect agreement with the steady-state current calculated with the master equation. Finally, we have also developed a heuristic method for calculating the average transfer time, which has allowed us to study the current up to a much larger system size than the methods using the density matrix. By doing so, we have further confirmed that the steady-state current is independent of dephasing up to a critical dephasing, $\gamma_\phi = W_{MIT} = 2$, which is independent of system size.

In coclusions we have found that: *i*) At the MIT, the current and the diffusion coefficient are independent of dephasing up to a critical value of γ_ϕ/Ω, which is independent of the system size; *ii*) in the metallic regime, for $W/\Omega < 2$, the transport efficiency decreases as dephaing increases; *iii*) in the localized regime, for $W/\Omega > 2$, the transport efficiency reaches a maximum when $\gamma_\phi/\Omega = W/\Omega$.

5.2 Perspectives

We are interested in understanding the origin of the noise independent transport found at the MIT. We want to answer the following question: whether the transport in the Harper model is independent of dephasing in the MIT because the motion is diffusive or because of the presence of a phase transition. In other words, is it true that when the motion is diffusive, we have a noise independent transport up to a critical dephasing independent of the system size? or is it due to the presence of the MIT? Of course, to study this question, it would be good to study other models that present an MIT, e.g., the Power-law Banded Random Matrix (PBRM) [45, 46] or other models that present diffusive motion, e.g., the Anderson quasi 1D model [47]. It would also be very interesting to study the 3D Anderson model [15, 48], which presents MIT.

Bibliography

[1] J. Schachenmayer, C. Genes, E. Tignone, and G. Pupillo, "Cavity-enhanced transport of excitons," *Physical review letters*, vol. **114**, no. 19, p. 196 403, 2015.

[2] J. Grad, G. Hernandez, and S. Mukamel, "Radiative decay and energy transfer in molecular aggregates: The role of intermolecular dephasing," *Physical Review A*, vol. **37**, no. 10, p. 3835, 1988.

[3] F. C. Spano, J. R. Kuklinski, and S. Mukamel, "Cooperative radiative dynamics in molecular aggregates," *The Journal of chemical physics*, vol. **94**, no. 11, pp. 7534–7544, 1991.

[4] R. Monshouwer, M. Abrahamsson, F. Van Mourik, and R. Van Grondelle, "Superradiance and exciton delocalization in bacterial photosynthetic light-harvesting systems," *The Journal of Physical Chemistry B*, vol. **101**, no. 37, pp. 7241–7248, 1997.

[5] M. Mohseni, P. Rebentrost, S. Lloyd, and A. Aspuru-Guzik, "Environment-assisted quantum walks in photosynthetic energy transfer," *The Journal of chemical physics*, vol. **129**, no. 17, 11B603, 2008.

[6] G. L. Celardo, F. Borgonovi, M. Merkli, V. I. Tsifrinovich, and G. P. Berman, "Superradiance transition in photosynthetic light-harvesting complexes," *The Journal of Physical Chemistry C*, vol. **116**, no. 42, pp. 22 105–22 111, 2012.

[7] D. Ferrari, G. Celardo, G. P. Berman, R. Sayre, and F. Borgonovi, "Quantum biological switch based on superradiance transitions," *The Journal of Physical Chemistry C*, vol. **118**, no. 1, pp. 20–26, 2014.

[8] E. Akkermans, A. Gero, and R. Kaiser, "Photon localization and dicke superradiance in atomic gases," *Physical review letters*, vol. **101**, no. 10, p. 103 602, 2008.

[9] E. Akkermans and A. Gero, "Cooperative effects in one-dimensional random atomic gases: Absence of single-atom limit," *EPL (Europhysics Letters)*, vol. **101**, no. 5, p. 54 003, 2013.

[10] T. Bienaimé, N. Piovella, and R. Kaiser, "Controlled dicke subradiance from a large cloud of two-level systems," *Physical review letters*, vol. **108**, no. 12, p. 123 602, 2012.

[11] R. Kaiser, "Quantum multiple scattering," *Journal of Modern Optics*, vol. **56**, no. 18-19, pp. 2082–2088, 2009.

[12] C. W. Beenakker, "Random-matrix theory of quantum transport," *Reviews of modern physics*, vol. **69**, no. 3, p. 731, 1997.

[13] S. Sorathia, F. Izrailev, V. Zelevinsky, and G. Celardo, "From closed to open one-dimensional anderson model: Transport versus spectral statistics," *Physical Review E*, vol. **86**, no. 1, p. 011 142, 2012.

[14] A. Ziletti, F. Borgonovi, G. Celardo, F. Izrailev, L. Kaplan, and V. Zelevinsky, "Coherent transport in multibranch quantum circuits," *Physical Review B*, vol. **85**, no. 5, p. 052 201, 2012.

[15] P. W. Anderson, "Absence of diffusion in certain random lattices," *Physical review*, vol. **109**, no. 5, p. 1492, 1958.

[16] C. M. Kropf, G. L. Celardo, C. Giannetti, and F. Borgonovi, "Electric-field assisted optimal quantum transport of photo-excitations in polar heterostructures," *Physica E: Low-dimensional Systems and Nanostructures*, p. 114 023, 2020.

[17] A. F. Van Loo, A. Fedorov, K. Lalumiere, B. C. Sanders, A. Blais, and A. Wallraff, "Photon-mediated interactions between distant artificial atoms," *Science*, vol. **342**, no. 6165, pp. 1494–1496, 2013.

[18] J. E. Avron, D. Osadchy, and R. Seiler, "A topological look at the quantum hall effect," *Physics today*, vol. **56**, no. 8, pp. 38–42, 2003.

[19] C. Albrecht, J. Smet, K. Von Klitzing, D. Weiss, V. Umansky, and H. Schweizer, "Evidence of hofstadter's fractal energy spectrum in the quantized hall conductance," *Physical Review Letters*, vol. **86**, no. 1, p. 147, 2001.

[20] R. J. Sharma, J. N. Bandyopadhyay, and T. G. Sarkar, "Self-similar spectrum in effective time independent hamiltonians for kicked systems," *arXiv preprint arXiv:1504.06090*, 2015.

[21] S. Y. Jitomirskaya, "Metal-insulator transition for the almost mathieu operator," *Annals of Mathematics*, pp. 1159–1175, 1999.

[22] A. Avila and S. Jitomirskaya, "The ten martini problem," *Annals of Mathematics*, pp. 303–342, 2009.

[23] J. Billy, V. Josse, Z. Zuo, A. Bernard, B. Hambrecht, P. Lugan, D. Clément, L. Sanchez-Palencia, P. Bouyer, and A. Aspect, "Direct observation of anderson localization of matter waves in a controlled disorder," *Nature*, vol. **453**, no. 7197, pp. 891–894, 2008.

[24] G. Roati, C. D'Errico, L. Fallani, M. Fattori, C. Fort, M. Zaccanti, G. Modugno, M. Modugno, and M. Inguscio, "Anderson localization of a non-interacting bose–einstein condensate," *Nature*, vol. **453**, no. 7197, pp. 895–898, 2008.

[25] N. C. Chávez, F. Mattiotti, J. Méndez-Bermúdez, F. Borgonovi, and G. L. Celardo, "Disorder-enhanced and disorder-independent transport with long-range hopping: Application to molecular chains in optical cavities," *arXiv preprint arXiv:2010.08060*, 2020.

[26] G. Vattay, S. Kauffman, and S. Niiranen, "Quantum biology on the edge of quantum chaos," *PloS one*, vol. **9**, no. 3, e89017, 2014.

[27] A. M. Lacerda, J. Goold, and G. T. Landi, "Dephasing enhanced transport in boundary-driven quasiperiodic chains," *arXiv preprint arXiv:2106.11406*, 2021.

[28] D. Dwiputra and F. P. Zen, "Environment-assisted quantum transport and mobility edges," *Physical Review A*, vol. 104, no. 2, p. 022 205, 2021.

[29] A. Szabó and U. Schneider, "Non-power-law universality in one-dimensional quasicrystals," *Physical Review B*, vol. **98**, no. 13, p. 134 201, 2018.

[30] S. Iyer, V. Oganesyan, G. Refael, and D. A. Huse, "Many-body localization in a quasiperiodic system," *Physical Review B*, vol. **87**, no. 13, p. 134 202, 2013.

[31] H. P. Lüschen, P. Bordia, S. Scherg, F. Alet, E. Altman, U. Schneider, and I. Bloch, "Observation of slow dynamics near the many-body localization transition in one-dimensional quasiperiodic systems," *Physical review letters*, vol. **119**, no. 26, p. 260 401, 2017.

[32] C. Soukoulis and E. Economou, "Localization in one-dimensional lattices in the presence of incommensurate potentials," *Physical Review Letters*, vol. **48**, no. 15, p. 1043, 1982.

[33] R. Shashidhara, "Driven aubry-andré-harper systems," Ph.D. dissertation, Birla Institute of Technology and Science, Pilani, 2017. [Online]. Available: https://www.cs.utexas.edu/~rajaths/thesis.pdf.

[34] G. Domıénguez-Castro and R. Paredes, "The aubry–andré model as a hobbyhorse for understanding the localization phenomenon," *European Journal of Physics*, vol. **40**, no. 4, p. 045 403, 2019.

[35] M. B. Plenio and S. F. Huelga, "Dephasing-assisted transport: Quantum networks and biomolecules," *New Journal of Physics*, vol. **10**, no. 11, p. 113 019, 2008.

[36] D. Manzano and E. Kyoseva, "An atomic symmetry-controlled thermal switch," *Scientific reports*, vol. **6**, no. 1, pp. 1–6, 2016.

[37] F. Mattiotti, "Interplay of cooperativity and noise: From light-harvesting complexes to quantum devices," Ph.D. dissertation, UNIVERSITÀ CATTOLICA DEL SACRO CUORE SEDE DI BRESCIA, 2017. [Online]. Available: http://www.infn.it/thesis/PDF/getfile.php?filename=11239-Mattiotti-specialistica.pdf.

[38] D. Manzano, "A short introduction to the lindblad master equation," *AIP Advances*, vol. **10**, no. 2, p. 025 106, 2020.

[39] E. Gholami and Z. M. Lashkami, "Noise, delocalization, and quantum diffusion in one-dimensional tight-binding models," *Physical Review E*, vol. **95**, no. 2, p. 022 216, 2017.

[40] P. Rebentrost, M. Mohseni, I. Kassal, S. Lloyd, and A. Aspuru-Guzik, "Environment-assisted quantum transport," *New Journal of Physics*, vol. **11**, no. 3, p. 033 003, 2009.

[41] C. Chuang, C. K. Lee, J. M. Moix, J. Knoester, and J. Cao, "Quantum diffusion on molecular tubes: Universal scaling of the 1d to 2d transition," *Physical review letters*, vol. **116**, no. 19, p. 196 803, 2016.

[42] Y. T Zhang, G. L. Celardo, F. Borgonovi, and L. Kaplan, "Opening-assisted coherent transport in the semiclassical regime," *Physical Review E*, vol. **95**, no. 2, p. 022 122, 2017.

[43] Y. Zhang, G. L. Celardo, F. Borgonovi, and L. Kaplan, "Optimal dephasing for ballistic energy transfer in disordered linear chains," *Physical Review E*, vol. **96**, no. 5, p. 052 103, 2017.

[44] J. M. Moix, M. Khasin, and J. Cao, "Coherent quantum transport in disordered systems: I. the influence of dephasing on the transport properties and absorption spectra on one-dimensional systems," *New journal of Physics*, vol. **15**, no. 8, p. 085 010, 2013.

[45] J. Mendez-Bermudez and I. Varga, "Scattering at the anderson transition: Power-law banded random matrix model," *Physical Review B*, vol. **74**, no. 12, p. 125 114, 2006.

[46] A. D. Mirlin, Y. V. Fyodorov, F.-M. Dittes, J. Quezada, and T. H. Seligman, "Transition from localized to extended eigenstates in the ensemble of power-law random banded matrices," *Physical Review E*, vol. **54**, no. 4, p. 3221, 1996.

[47] V. Gasparian and E. Cuevas, "Localization length in the quasi one-dimensional disordered system revisited," *Solid state communications*, vol. **164**, pp. 11–15, 2013.

[48] A. Lagendijk, B. Van Tiggelen, and D. S. Wiersma, "Fifty years of anderson localization," *Phys. Today*, vol. **62**, no. 8, pp. 24–29, 2009.

Appendix A

Purity

In quantum physics, a quantum state is a mathematical entity that provides a probability distribution for the outcomes of each possible measurement in a system. A mixture of quantum states is again a quantum state. Quantum states that cannot be written as a mixture of other states are called pure quantum states, while all other states are called mixed quantum states.

A pure quantum state is a state which a single ket vector can describe. A mixed quantum state is a statistical ensemble of pure states. In contrast, a mixed state cannot be described with a single ket vector. Instead, it is described by a associated density matrix, usually denoted ρ. Note that density matrices can describe both mixed and pure states.

A simple criterion for checking whether a density matrix describes a pure or mixed state is using

$$\gamma \equiv \sum_{i,j=1}^{N} \rho_{i,j}^{2}\,, \tag{A.1}$$

when the trace is equal to 1, the density matrix describes a pure state. Otherwise, the density matrix describes a mixed state.

Figure. A.1, we show the behavior of the purity as a function of time for different values of γ_ϕ for different values of W/Ω in a system size of $N = 100$. To obtain Fig. A.1 we consider a wave packet initially concentrated in the center of the chain. Then we solve the Master Equation (see Eq. 3.1) with Haken-Strobl pure dephasing (see Eq. 3.4). Finally, we extract the purity of the complete system using the Eq. A.1. In a general way, we can appreciate that the value of W/Ω and γ_ϕ/Ω are unimportant, the system starts having a pure state, and it ends up having equiprobable mixed states, which take the value of $N/1$.

Also, the time needed for the system to be affected by γ_ϕ/Ω decreases up to a certain value of γ_ϕ/Ω. Overcoming that value, the system takes more time to be affected by γ_ϕ/Ω. This figure is organized into three panels. Panel (a) is for $W/\Omega = 0$; metallic regime. Panel (b) refers is for $W/\Omega = 0$; MIT. Panel (c) is for $W/\Omega = 20$; insulating regime. In particular, in panel (b), we notice that for a value of $\gamma_\phi/\Omega = 2$, the purity decay curves become overlap, which can be interpreted as the system being independent of γ_ϕ/Ω, up to a critical value of γ_ϕ/Ω, after a period of time.

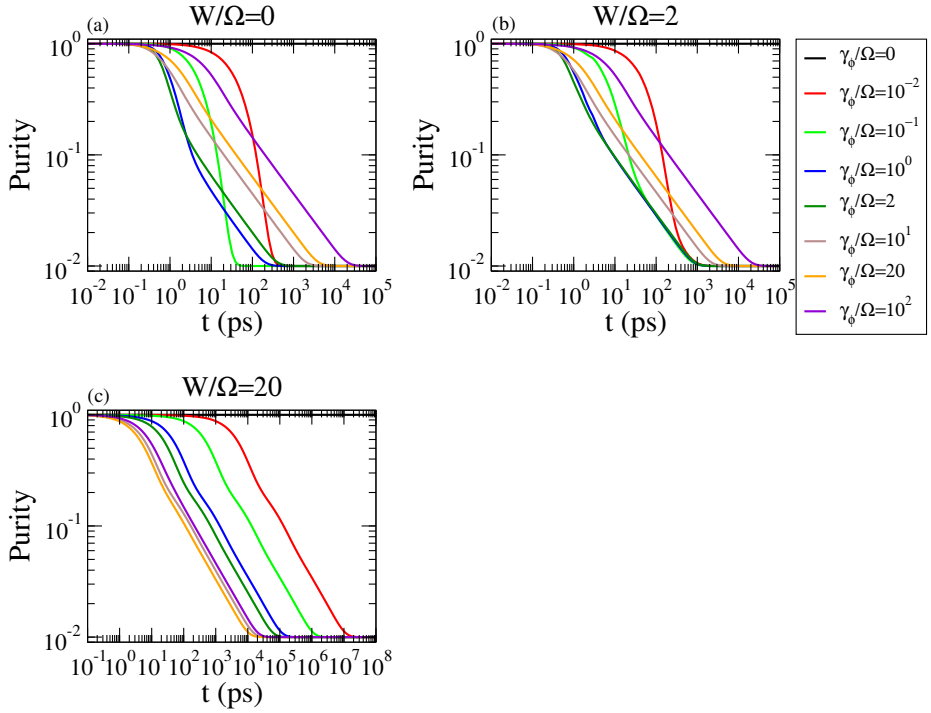

Figure A.1: Purity as a function of time for different values of W/Ω and γ_ϕ/Ω. This figure is organized in three panels; each one is for a different value of W/Ω. Panel (a) is for $W/\Omega = 0.0$, panel (b) is for MIT, and panel (c) is for $W/\Omega = 20$. All the curves are obtained using Eq. A.1. The initial condition is given by a wave packet initially concentrated in the center of the chain. The parameters are: $N = 100$, $\Omega = 1cm^{-1}$, $\beta = (\sqrt{5}-1)/2$ and $\hbar = 5.29cm^{-1}ps$.

Figure A.2 is a comparison of the purity between the three regimes. Here, we show that in the metallic regime is where the purity decays the fastest, while in the insulating regime it decays the slowest. In the metallic-insulating regime, purity decays somewhere between the other two regimes. This is why some people have thought that the MIT is an excellent point to transport because the transport is not inadequate and purity decay is not

so fast. In other words, the system can transport well, retaining some purity even in the presence of dephasing.

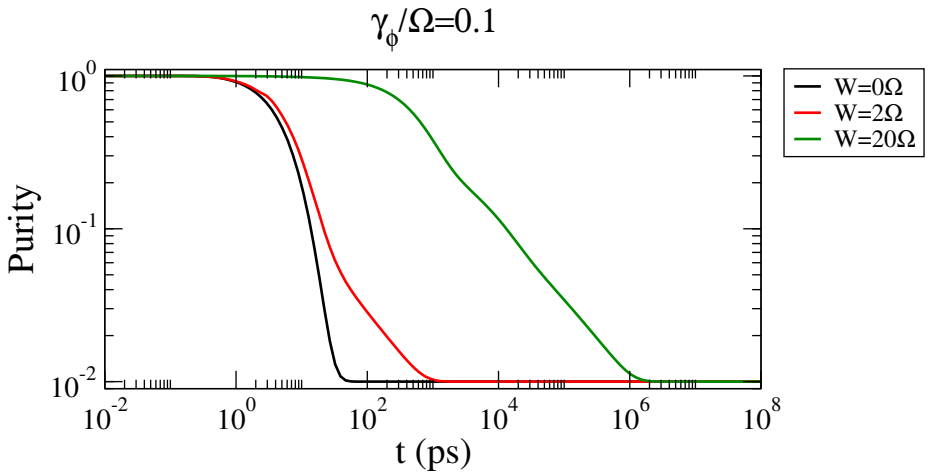

Figure A.2: Purity as a function of time for the Harper model with Haken-Stobl dephasing in different values of W/Ω and γ_ϕ/Ω. This figure is a comparison of the three regimes of the previous figure for a fix $\gamma_\phi = 0.1$. All the curves are obtained using Eq. A.1. The initial condition is given by a wave packet initially concentrated in the center of the chain. The parameters are: $N = 100$, $\Omega = 1cm^{-1}$, $\beta = (\sqrt{5}-1)/2$ and $\hbar = 5.29cm^{-1}ps$.

Appendix B

Coherence length

The coherence length tells us in how many sites the excitation, in presence of dephasing, is spreading. Then, when the excitation is evenly distributed in a classical way on all the sites, the coherence length is one. Here we study the time evolution of the coherence length, defined in terms of the density matrix as:

$$L_\rho = \frac{\left(\sum_{i,j=1}^{N} |\rho_{ij}|\right)^2}{N \sum_{i,j=1}^{N} |\rho_{ij}|^2} \,. \tag{B.1}$$

Figure B.1, we show the behavior of the coherence length as a function of time for different values of γ_ϕ for different values of W/Ω in a system size of $N = 100$. To obtain Fig. B.1, we consider a wave packet initially concentrated in the center of the chain. Then we solve the Master Equation (see Eq. 3.1) with Haken-Strobl pure dephasing (see Eq. 3.4). Finally, we extract the coherence length of the complete system using the Eq. B.1. This figure is organized into three panels. Panel (a) is for $W/\Omega = 0$; metallic regime. Panel (b) refers is for $W/\Omega = 0$; MIT. Panel (c) is for $W/\Omega = 20$; insulating regime.

Figure B.2, we show that the excitation spreads quickly in the metallic regime, so this is why the coherence grows very fast but decreases to one very fast as well. The excitation does not spread quickly in the insulating regime, so the coherence is very little and slowly grows to 1. In the MIT, even if the coherence length is not so high, it took more time to go to 1.

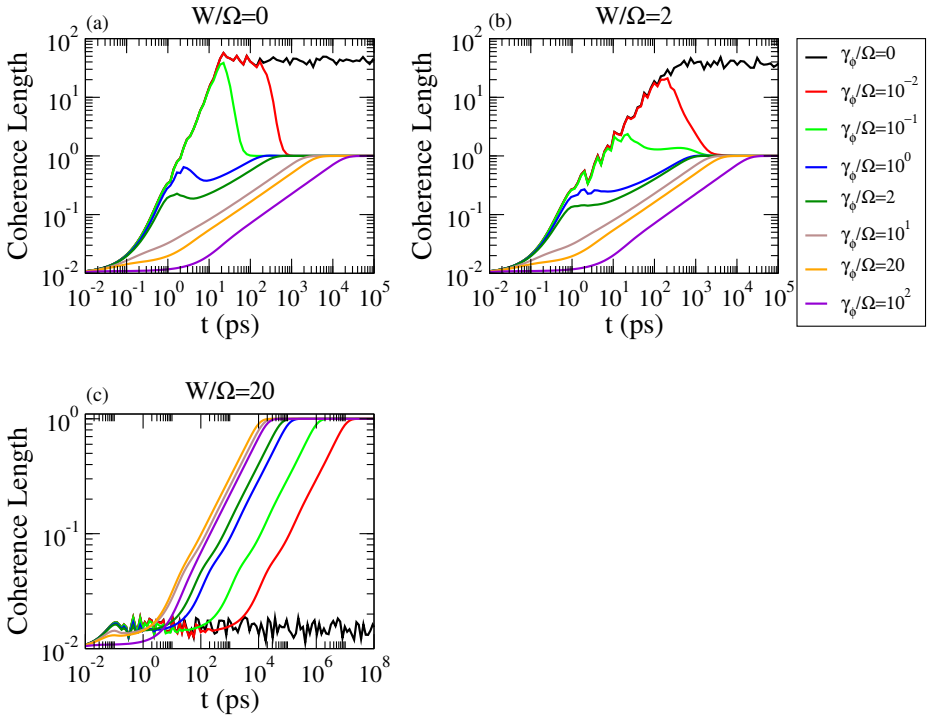

Figure B.1: Coherence length as a function of time for Harper model with Haken-Stobl dephasing for different values of W/Ω and γ_ϕ. This figure is organized in three panels; each one is for a different value of W/Ω. Panel (a) is for $W/\Omega = 0.0$, panel (b) is for MIT, and panel (c) is for $W/\Omega = 20$. All the curves have been obtained using Eq. B.1. The initial condition is given by a wave packet initially concentrated in the center of the chain. The parameters are: $N = 100$, $\Omega = 1cm^{-1}$, $\beta = (\sqrt{5}-1)/2$ and $\hbar = 5.29cm^{-1}ps$.

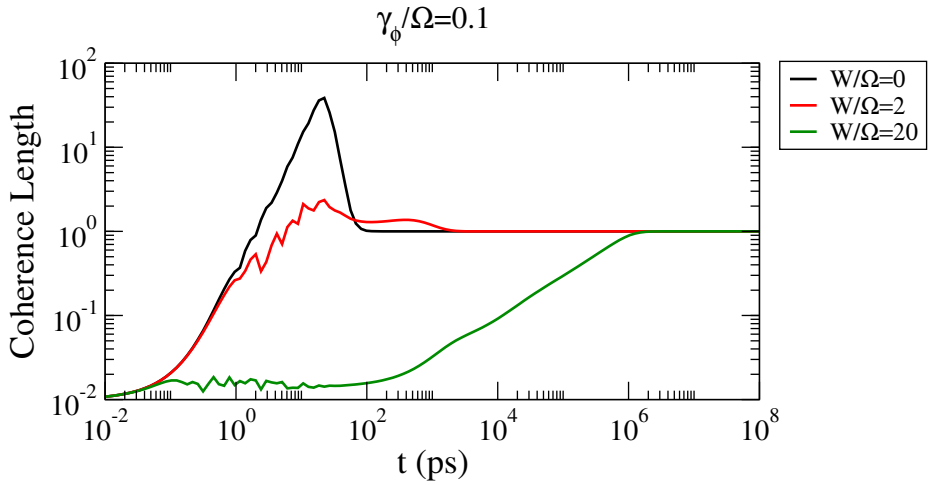

Figure B.2: Coherence length as a function of time for Harper model with Haken-Stobl dephasing in different values of W/Ω for different values of γ_ϕ/Ω. This figure is a comparison of the three regimes of the previous figure for a fix $\gamma_\phi = 0.1$. All the curves are obtained using Eq. A.1. The initial condition is given by a wave packet initially concentrated in the center of the chain. The parameters are: $N = 100$, $\Omega = 1cm^{-1}$, $\beta = (\sqrt{5}-1)/2$ and $\hbar = 5.29cm^{-1}ps$.

Appendix C

Method for solving the Master Equation

To study the properties of an open system in this thesis work, we use the Master Equation approach since it correctly describes the dynamics produced by an open system. The master equation has the advantage of always being a linear equation considering that it can be written in Lindblad form.

We solve the Master Equation as Mattiotti [37]. For this procedure, we start by introducing an alternative form of the master equation (Eq. 3.1). We want to represent the action generated on the density matrix as the application of a matrix to a vector. The master equation is the time derivative of the density matrix equated to applying a linear superoperator to the same density matrix. If the density matrix represents a vector, it can be viewed as applying a suitably transformed matrix to a vector. The new representation produces a system of N^2 equations of motion.

The new representation of the density matrix, which is an $N \times N$ matrix, consists of putting one column after another, so that

$$\vec{\rho}^{T} = (\rho_{1,1}, \rho_{1,2}, \cdots, \rho_{1,N}, \rho_{2,1}, \rho_{22}, \cdots, \rho_{N,N})\,. \tag{C.1}$$

Now analogous to the density vector, we construct an $N^2 \times N^2$ $\mathcal{F}_{a,b}$ matrix that allows us to write the master equation in general form

$$\frac{d\vec{\rho}_a}{dt} = \sum_{b=1}^{N^2} \mathcal{F}_{a,b}\vec{\rho}_b \tag{C.2}$$

where the indices a and b run from 1 to N^2. The linearity of the operator is preserved so that the $\mathcal{F}_{ab}$ matrix can be constructed as the sum of five terms: the two parts of the commutator and the three dissipators.

The formal solution for Eq. C.2 is

$$\vec{\rho}(t) = e^{\mathcal{F}t}\vec{\rho}(0)\,. \tag{C.3}$$

To solve Eq. C.3 above, we must diagonalize $\mathcal{F}$. If F is diagonalizable, it is always true that

$$\mathcal{F} = VDV^{-1} \tag{C.4}$$

where V is a matrix in which its columns are the right eigenvectors of $\mathcal{F}$ and D is the diagonal form of $\mathcal{F}$, in which the diagonal elements $\lambda_1, \cdots, \lambda_N^2$ are the eigenvalues of $\mathcal{F}$.

Substituting Eq. C.4 in Eq. C.3 and expanding the exponential n a power series, we have

$$\vec{\rho}(t) = e^{VDV^{-1}t}\vec{\rho}(0) = \sum_{n=0}^{\infty} \frac{(VDV^{-1})^n t^n}{n!}\vec{\rho}(0). \tag{C.5}$$

Now we note that

$$(VDV^{-1})^n = VDV^{-1}VDV^{-1}\cdots VDV^{-1} = VD^nV^{-1}\,, \tag{C.6}$$

notice that $VV^{-1} = I$, and I is the identity. So, we can rewrite Eq. C.5 as

$$\vec{\rho}(t) = V\sum_{n=0}^{\infty} \frac{(Dt)^n}{n!}V^{-1}\vec{\rho}(0) = Ve^{Dt}V^{-1}\vec{\rho}(0), \tag{C.7}$$

since D is diagonal, $e^{Dt} = e^{\lambda_1 t}e^{\lambda_2 t}\cdots e^{\lambda_{N^2} t}$. So we have obtained the analytical solution of Eq. C.2 at the time t

$$\vec{\rho}_a(t) = \sum_{b=1}^{N^2}\sum_{c=1}^{N^2} V_{a,b}e^{\lambda_b t}V^{-1}_{b,c}\vec{\rho}_c(0). \tag{C.8}$$

This method gives an exact solution for any time t, being particularly useful if the time interval to be calculated is long. The disadvantage of using this method is that it requires solving a non-Hermitian $N^2 \times N^2$ matrix. Obtaining the eigenvalues, eigenvectors and the inverse matrix of the right eigenvectors are operations that can be performed numerically but can be very expensive when the size of the system is large. In addition,

repeating the calculation C.8 for N^2 times to obtain the complete density matrix at t further increases the computational time.

Appendix D

Different methods to obtain diffusion coefficient

To determine the accuracy of Eq. 4.11, we make a comparison between the diffusion coefficient D obtained from the Master Equation method (Eq. 3.1) and the Jianshu method (Eq. 4.11). To obtain D from the Master Equation method, we solve Eq. 3.1 and take the variance using Eq. 4.12. Then, we fit the linear part of the variance of the spreading wave packet as $y = a_1 x + a_0$, where $D = a_1/2$.

Figure D.1 is organized by columns and rows. Each row corresponds to a different value of the dephasing strength. The left column refers to the dynamics of the wave packet spreading in the presence of dephasing for different values of W/Ω. We consider a wave packet initially concentrated in the center of the chain as an initial condition. The vertical dashed lines correspond to $t = \hbar/W$. The vertical dash-dotted line black lines correspond to $t = \hbar/\gamma_\phi$. The horizontal dotted green line is the saturation value $\sigma_{sat} = N^2/12$. The oblique dashed double dotted lines correspond to the diffusive motion $\sigma^2 = 2Dt$ (Eq. 4.16), where the diffusion coefficient has been obtained from Eq. 4.11. The left panel is for the diffusion coefficient as a function of dephasing for different values of W/Ω. To obtain the figures of this column, we use Eq. 4.11. The vertical dash-dotted black line corresponds to $\gamma_\phi = 4\Omega/N$. The marks refer to the value of D obtained using the Master Equation method.

$\gamma_\phi=10^{-5}$

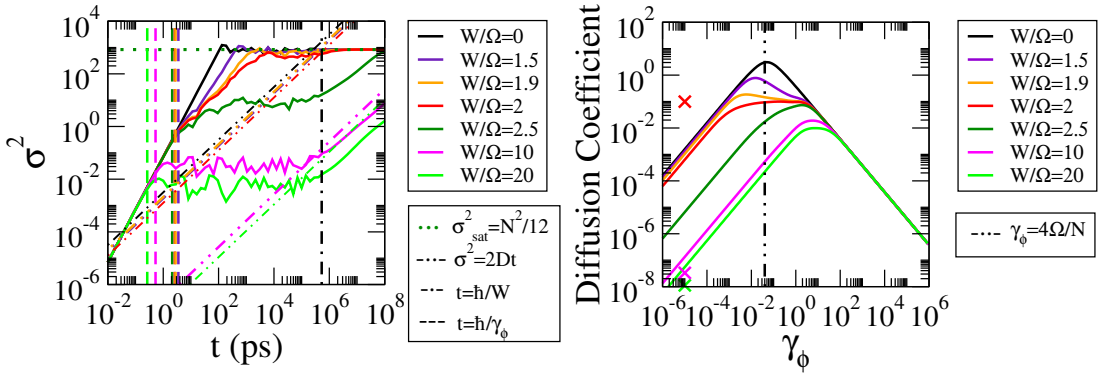

$\gamma_\phi=10^{-4}$

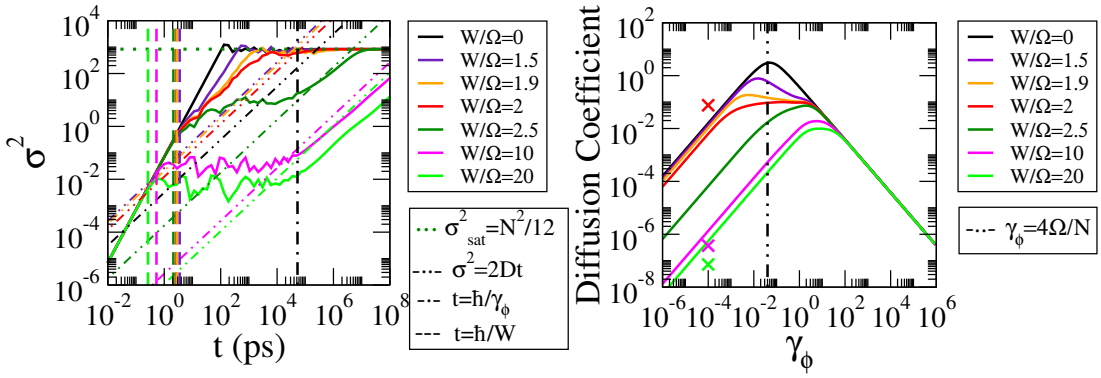

$\gamma_\phi=10^{-3}$

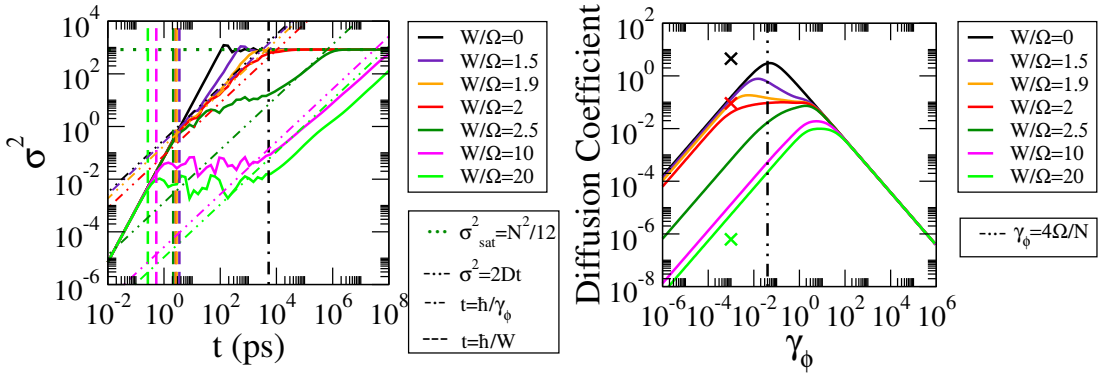

$\gamma_\phi=10^{-2}$

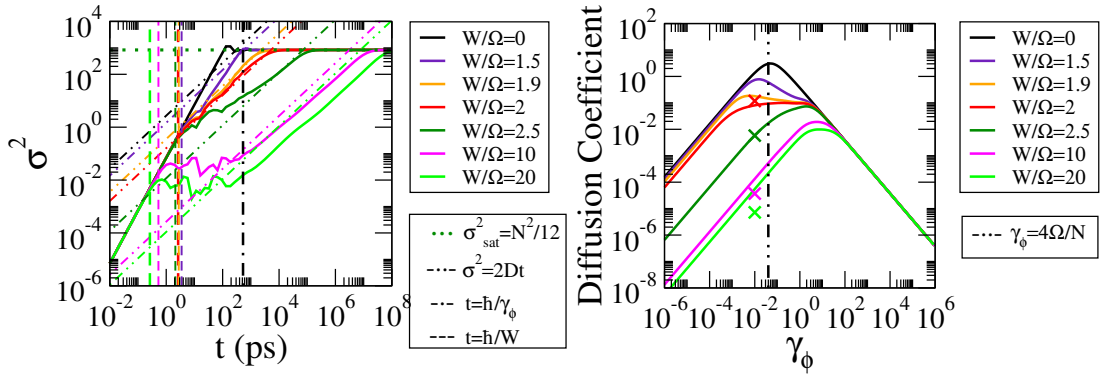

$\gamma_\phi=10^{-1}$

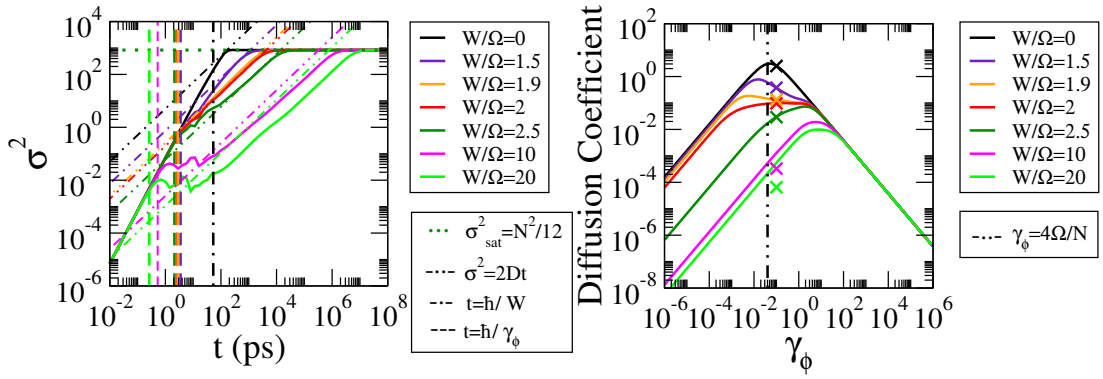

$\gamma_\phi=1$

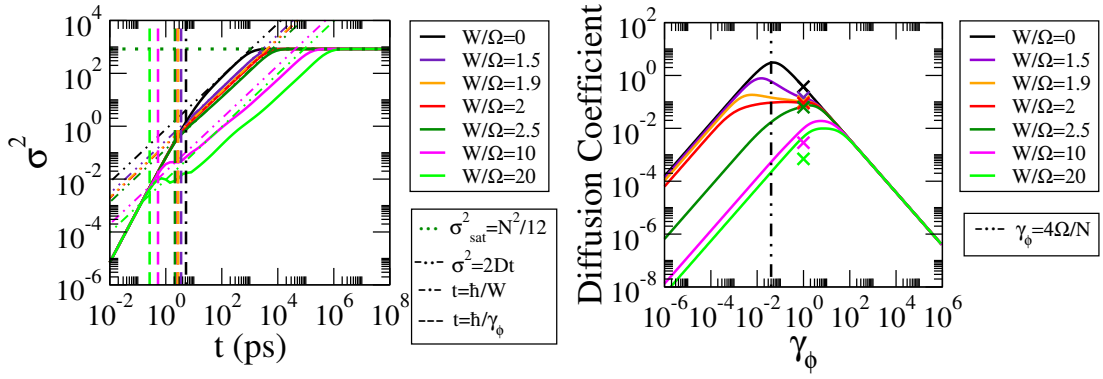

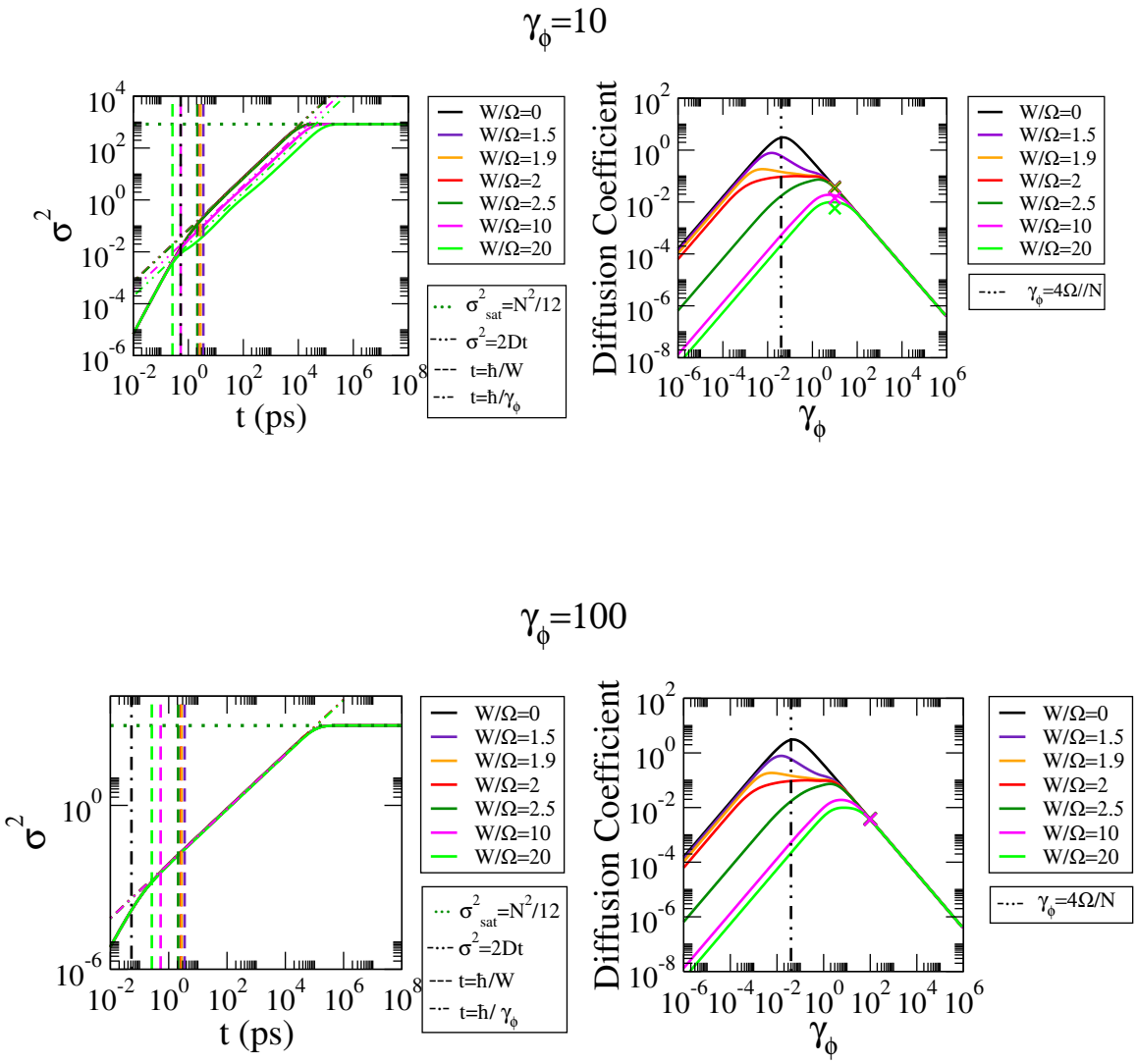

Figure D.1: The left panel; dynamics of a wave packet initially concentrated in the central site of the chain for different values of W/Ω and dephasing. For this, we solve Eq. 3.1 with Eq. 3.4 and use the Eq. 4.12. The vertical dashed lines correspond to $t = \hbar/W$. The vertical dash-dotted line black line corresponds to $t = \hbar/\gamma_\phi$. The horizontal dotted green line is the saturation value $\sigma_{sat} = N^2/12$. The oblique dash double dotted lines correspond to a diffusive motion $\sigma^2 = 2Dt$ (Eq. 4.16), where the diffusion coefficient has been obtained from Eq. 4.11. The right panel; diffusion coefficient as a function of dephasing for different values of W/Ω. For this, we use the Eq. 4.11. The marks refer to the value of D obtained from the dynamics. The vertical dash double dotted black line corresponds to $\gamma_\phi = 4\Omega/N$. The parameters are: $\Omega = 1cm^{-1}$, $\beta = (\sqrt{5}-1)/2$, and $\hbar = 5.29cm^{-1}ps$.